



Published in final edited form as:

Neurobiol Dis. 2021 January ; 148: 105175. doi:10.1016/j.nbd.2020.105175.

The BDNF Val66Met polymorphism (rs6265) enhances dopamine neuron graft efficacy and side-effect liability in rs6265 knock-in rats

Natosha M. Mercado^a, Jennifer A. Stancati^a, Caryl E. Sortwell^{a,b}, Rebecca L. Mueller^a, Samuel A. Boezwinkle^c, Megan F. Duffy^a, D. Luke Fischer^a, Ivette M. Sandoval^{a,b}, Fredric P. Manfredsson^{a,b}, Timothy J. Collier^{a,b}, Kathy Steece-Collier^{a,b,*}

^aDepartment of Translational Neuroscience, College of Human Medicine, Michigan State University, Grand Rapids, MI 49503, USA

^bHauenstein Neuroscience Center, Mercy Health Saint Mary's, Grand Rapids, Michigan 49503, USA

^cCollege of Literature, Science, and the Arts, University of Michigan, Ann Arbor, Michigan 48109, USA

Abstract

Prevalent in approximately 20% of the worldwide human population, the rs6265 (also called 'Val66Met') single nucleotide polymorphism (SNP) in the gene for brain-derived neurotrophic factor (*BDNF*) is a common genetic variant that can alter therapeutic responses in individuals with Parkinson's disease (PD). Possession of the variant Met allele results in decreased activity-dependent release of BDNF. Given the resurgent worldwide interest in neural transplantation for PD and the biological relevance of BDNF, the current studies examined the effects of the rs6265 SNP on therapeutic efficacy and side-effect development following primary dopamine (DA) neuron transplantation. Considering the significant reduction in BDNF release associated with rs6265, we hypothesized that rs6265-mediated dysfunctional BDNF signaling contributes to the limited clinical benefit observed in a subpopulation of PD patients despite robust survival of grafted DA neurons, and further, that this mutation contributes to the development of aberrant graft-induced dyskinesias (GID). To this end, we generated a CRISPR knock-in rat model of the rs6265 *BDNF* SNP to examine for the first time the influence of a common genetic polymorphism on graft survival, functional efficacy, and side-effect liability, comparing these parameters between wild-type (Val/Val) rats and those homozygous for the variant Met allele (Met/Met). Counter to our hypothesis, the current research indicates that Met/Met rats show enhanced graft-associated therapeutic efficacy and a paradoxical enhancement of graft-derived neurite outgrowth compared to wild-type rats. However, consistent with our hypothesis, we demonstrate that the rs6265

This is an open access article under the CC BY-NC-ND license (<http://creativecommons.org/licenses/by-nc-nd/4.0/>).

*Corresponding author at: Department of Translational Neuroscience, College of Human Medicine, Michigan State University, 400 Monroe Ave NW, Grand Rapids, MI 49503, USA. collie68@msu.edu (K. Steece-Collier).

Supplementary data to this article can be found online at <https://doi.org/10.1016/j.nbd.2020.105175>.

Declaration of Competing Interest
None.

genotype in the host rat is strongly linked to development of GID, and that this behavioral phenotype is significantly correlated with neurochemical signatures of atypical glutamatergic neurotransmission by grafted DA neurons.

Keywords

Parkinson's disease; Neural grafting; Val66Met; Val68Met; rs6265; BDNF

1. Introduction

While there are various therapeutic options for individuals with Parkinson's disease (PD), these therapies do not work uniformly well in all patients and eventually most are plagued with waning efficacy and significant side-effects as the disease progresses. Indeed, there is growing consensus surrounding the contention that PD is a complex and heterogeneous neurodegenerative process, the molecular underpinnings and clinical presentation of which vary greatly among individuals. For example, while the mainstay pharmacotherapy for PD, oral levodopa, is generally effective in treating the motor symptoms of PD, the clinical response can be variable. In accordance, a retrospective analysis of the 'Earlier versus Later Levodopa Therapy in Parkinson Disease' (ELL-DOPA) study reported that early-stage PD subjects receiving equivalent levodopa doses experienced a magnitude of response ranging from a 100% improvement to a 242% worsening as assessed with the United Parkinson's Disease Rating Scale part III (UPDRS-III, motor subscore) (Hauser et al., 2009). This inherent heterogeneity is a significant hindrance to the overall therapeutic goal of "implementing safe, effective, and individually tailored interventions with minimal complications" (Sieber et al., 2014) for those afflicted with PD.

In an effort to increase the number of therapeutic options for persons afflicted with PD, for more than three decades experimental therapies in the field of regenerative medicine have examined means of restoring lost dopamine (DA) terminals within the striatum, whether through grafting replacement neurons (primary DA neurons or stem cells) (Stoker et al., 2017; Towns, 2017; Barker and Consortium, 2019) or vector-mediated delivery of trophic factors to induce terminal sprouting from remaining DA neurons (Tenenbaum and Humbert-Claude, 2017; Olanow et al., 2015). The approach that has had most success clinically is embryonic ventral mesencephalic (VM) DA neuron engraftment into the caudate/putamen, which clearly shows efficacy in a subpopulation of individuals with PD (e.g., (Stoker et al., 2017; Olanow et al., 2009; Steece-Collier et al., 2012)). As recently reviewed (Stoker et al., 2017; Collier et al., 2019), despite strong biological rationale, a lack of consistent benefit and the occurrence of significant graft-derived side-effects (Piccini et al., 2005; Freed et al., 2001; Hagell et al., 2002; Olanow et al., 2003; Soderstrom et al., 2008; Lindvall, 2015) have tempered enthusiasm regarding the clinical utility of DA neuron grafting for PD. However, after more than a decade of refinement, more rigorously designed grafting studies are ongoing or planned for the near future (e.g., (Barker and Consortium, 2019), Clinical Trial Identifiers [NCT01898390](#), [NCT03309514](#), [NCT03119636](#), [NCT04146519](#)).

While the field has gained an understanding of the role of *global* risk factors (e.g., disease severity, host age, etc.), the role that specific *genetic* risk factors might play in neural transplantation studies remains entirely unexplored. With this in mind, one approach to deconstructing the complexity of PD and response to therapy is the identification of common genetic variants that influence these variables in order to predict disease characteristics and tailor treatments to those most effective for subpopulations of patients. We recently identified one genetic variant which may prove useful in this regard. Specifically, we have found that the single nucleotide polymorphism (SNP) rs6265 in the brain-derived neurotrophic factor gene (*BDNF*) reduces the therapeutic efficacy of oral levodopa in two distinct cohorts of PD patients (Sortwell et al., 2017; Fischer et al., 2020). The rs6265 SNP, which is also commonly known as ‘Val66Met’ results in a methionine (Met) amino acid substitution for valine (Val) at codon 66. The rs6265 Met allele variant has a prevalence of 15–20% in the general worldwide population, though estimates vary between studies and between populations (e.g., the estimated prevalence of the variant allele in African communities is <5%, whereas in East Asian populations, this estimate is as high as 72%) (dbSNP, 2020; Petryshen et al., 2010). Both the heterozygous major allele (Val/Met) and homozygous minor allele (Met/Met) of the *BDNF* SNP result in a dose dependent (homozygous > heterozygous) decreased activity-dependent release of BDNF by disrupting BDNF transport and packaging into secretory vesicles, whereas constitutive levels of BDNF secretion remain unaffected (Chen et al., 2006; Egan et al., 2003; Wu et al., 2010; Baj et al., 2013; Mallei et al., 2015). Importantly, the majority of BDNF in the adult brain is released from neurons via the regulated secretory pathway; therefore, the impact of the rs6265 SNP leads to a significant decrease in available BDNF (Chen et al., 2006; Egan et al., 2003) in approximately 15–20% of the general human population.

The rs6265 SNP is not associated with PD incidence (Mariani et al., 2015). However, based on the prevalence of this SNP, the known influential role of BDNF on embryonic VM grafts (Hoglinger et al., 2001; Yurek et al., 1996; Yurek et al., 1998; Zhou et al., 1997), and the critical role that BDNF plays in promoting dendritic spine growth and formation of synapses in the central nervous system (Adachi et al., 2014), we hypothesized that this genetic risk factor might underlie the variability in clinical response to DA neuron grafting in PD patients. To examine this hypothesis, we generated a knock-in rat model of the human rs6265 *BDNF* variant and used this novel tool to characterize, for the first time, the effects of this polymorphism on the function and synaptic integration of new DA terminals into the parkinsonian striatum using neural grafting as a model system. Specifically, we were interested in testing the overarching hypothesis that the rs6265 *BDNF* variant expressed by the graft recipient is an unrecognized contributor to the lack of behavioral efficacy despite robust survival of grafted neurons and/or induction of graft-induced dyskinesias (GID) reported in a subpopulation of PD patients (Piccini et al., 2005; Freed et al., 2001; Hagell et al., 2002; Olanow et al., 2003; Soderstrom et al., 2008; Lindvall, 2015). To test this hypothesis we have compared rats homozygous for this SNP (Met/Met), the genotype that would produce the largest reduction in BDNF release, with wild-type (Val/Val) rats to maximize the chances of observing any potential effect associated with the Met allele.

In the current studies, we shifted focus from the grafted cells to the environment into which the cells are grafted. In this context, we provide novel and compelling evidence that,

contrary to one aspect of our hypothesis, parkinsonian rats homozygous for the Met Met allele show a paradoxical enhancement of grafted DA neurite outgrowth and graft-derived efficacy despite equivalent survival of grafted DA neurons compared to wild-type rats. This enigmatic finding of enhanced functional recovery in Met allele carriers is corroborated by previous clinical and preclinical evidence (Krueger et al., 2011; Qin et al., 2014; Fischer et al., 2018). However, consistent with our hypothesis, only the Met/Met subjects exhibited an induction of GID behavior demonstrating for the first time that an individuals' genetic profile, specifically the rs6265 SNP, is uniquely linked to development of aberrant behavioral side-effects following DA neuron grafting. While the mechanism(s) underlying these findings associated with the Met/Met genotype remain uncertain, the current investigations described here suggest that an atypical neurochemical phenotype of the grafted neurons and atypical graft-host circuitry may contribute to GID expression.

2. Materials and methods

2.1. Animals

Rats were derived from a heterozygous female Sprague-Dawley rat (CD® International Genetic Standardization Program, Charles River Laboratories, Wilmington, MA, USA) carrying the valine to methionine polymorphism (Val68Met) in the rat *Bdnf* gene (GenBank: [NM_001270630](#); Ensembl: ENSRNOG00000047466). Note that rats have two additional threonine amino acids at positions 57 and 58, making the rat Val68Met equivalent to the human Val66Met SNP; the rat *Bdnf* gene is 96.8% homologous with the human *BDNF* gene (BLAST queries: P23560 and P23363). This *Bdnf* knock-in rat model was generated, under contract and guidance by our group, by Cyagen Biosciences (Santa Clara, CA, USA) using CRISPR/Cas-mediated homologous recombination (Supplementary Fig. 1). Cas9, guide RNA (gRNA) targeting vector (target sequence: 5'-GCACGTGATCGAAGAGCTGCTGGATG-3'; gRNA sequence: 3'-GCAGGGACCGACTGTGAAAACCTCGTGAC-5'), and a Val68Met template donor (template sequence: 5'-ACGTCCCTGGCTGACACTTTTGAGCACATGATC GAAGAGCTGCTGGATGA-3') were injected into zygotes to generate the Val68Met Sprague-Dawley rat (Supplementary Fig. 1a,b). Polymerase chain reaction followed by DNA sequencing (DNA sequencing primer: 5'-AGGTCTGAAATTACAAGCAGATGG-3') were performed to confirm that the founder female rat was carrying the valine to methionine polymorphism (Supplementary Fig. 1c,d). Next, the founder female was bred once with a wild-type Val68Val male Sprague-Dawley rat to generate heterozygous Val68Met offspring of both sexes. Subsequent breeding of heterozygous Val68Met rats produced offspring of all genotypes (wild-type Val68Val, heterozygous Val68Met, and homozygous Met68Met) for colony maintenance and experimentation. Offspring were genotyped using a custom Taqman® SNP genotyping assay (Supplementary Fig. 1e). Furthermore, we confirmed that *in vitro* BDNF release was reduced in cultured neurons from Met68Met rats without altering total BDNF brain tissue content (Supplementary Fig. 2). Colonies of Val68Val, Val68Met, and Met68Met rats were established with no breeding issues. Both heterozygous Val68Met and homozygous Met68Met rats are viable for at least 22 months, the longest we have aged them.

For the current experiments, mature adult male rats (6 m.o. at time of lesion, $N=24$ rs6265 rats, $N=23$ wild-type rats) were produced in-house within our Val68Met colony as described above. In these initial proof-of-principle studies, wild-type (Val68Val) and homozygous SNP (Met68Met) rats were used to maximize the chances of observing any potential effect associated with the variant allele. Rats were housed on a 12 hour light/dark cycle (lights on at 06:00) and given access to food and fresh water *ad libitum*. Rats were housed two per cage until initiation of levodopa treatment and dyskinesia rating when they were then individually housed with environmental enrichment to allow accurate behavioral assessment in their home cage. All experimental procedures were approved by the Michigan State University Institutional Animal Care & Use Committee. Further, “principles of laboratory animal care” (NIH publication No. 86–23, revised 1985) were followed, as well as specific national and international laws in accordance with the ethical standards established by the 1964 Declaration of Helsinki and its later amendments or comparable ethical standards.

2.2. Experimental design overview

Briefly, as shown in the experimental timeline (Fig. 1) and detailed in the paragraphs below, rats were rendered unilaterally parkinsonian via stereotaxic injection of 6-hydroxydopamine (6-OHDA). Two weeks following 6-OHDA surgery, lesion success was verified with amphetamine-induced rotational behavior. Two weeks later, rats were primed with daily levodopa to induce stable levodopa-induced dyskinesias (LID). After 5 weeks of levodopa priming, all rats received an intrastriatal graft of embryonic VM DA neurons from wild-type (Val68Val) rats or a cell-free sham graft. Levodopa was withdrawn for one week following graft surgery, after which levodopa treatment was reinitiated. Parkinsonian rats were evaluated for amelioration of LID behavior for 9 weeks following engraftment. At 7 weeks post-engraftment, amphetamine-induced rotational behavior was assessed once again as a secondary measure of graft function. As an indicator of graft dysfunction, GID were evaluated following the last week of LID assessment (i.e., 10 weeks post-grafting). Following the conclusion of the study, all rats were genotyped to confirm Val68Met SNP genotype.

2.3. Nigrostriatal 6-OHDA lesion surgery

Rats were anesthetized with inhalant isoflurane (2–3%; Sigma, St. Louis, MO, USA) and secured in a stereotaxic frame (David Kopf Instruments, Tujunga, CA, USA). Each rat received 2 μ l of 6-OHDA (5mg/ml) using a 5 μ l Hamilton syringe with a 26-gauge needle. 6-OHDA was administered at a flow rate of 0.5 μ l/min into the substantia nigra pars compacta (SNc; 4.8 mm posterior, 1.7 mm lateral, 8.0 mm ventral, relative to bregma) and the medial forebrain bundle (MFB; 4.3 mm posterior, 1.6 mm lateral, 8.4 mm ventral, relative to bregma). These lesioning parameters result in greater than 90% SNc DA neuron death, which is required in this model to produce reliable LID and significant parkinsonian motor deficits (Zhang et al., 2013; Konradi et al., 2004; Morin et al., 2014; Cenci and Crossman, 2018). After surgery completion, rats received carprofen (as Rimadyl®; 5 mg/kg) as analgesic treatment. Nigral lesion status was confirmed histologically postmortem with medial terminal nucleus DA cell enumeration, as described previously (Gombash et al., 2014).

2.4. Amphetamine-induced rotational behavior

Amphetamine-induced rotational behavior is a reliable measure of nigrostriatal DA depletion and graft function (e.g., (Soderstrom et al., 2008; Collier et al., 2015; Collier et al., 1999; Dunnett et al., 1981)). Accordingly, amphetamine-induced rotational asymmetry was assessed 2 weeks following lesion surgery to confirm successful lesion status, and again at 7 weeks post-engraftment as a secondary endpoint to assess DA neuron graft function per (Collier et al., 2015). Rats were injected with amphetamine sulfate [5 mg/kg, intraperitoneal (i.p.)] and rotational behavior was monitored using an automated Rotometer System (TSE-Systems, Chesterfield, MO, USA) for 90 min. Rats rotating at a rate of 7 ipsilateral turns per minute over 90 min 2 weeks post-lesion were included for further study.

2.5. Levodopa administration

Beginning 4 weeks after 6-OHDA surgery, rats were primed for 5 weeks with once daily (M-Fr) injections of levodopa plus benserazide [12 mg/kg, 1:1; subcutaneous (s.c.)]. Levodopa was withdrawn for one week following graft surgeries to prevent any potential toxic interaction of the drug with grafted cells (Collier et al., 2015; Steece-Collier et al., 1990) and was then reinitiated and continued daily (M-Fr) throughout the remainder of the experiment (Fig. 1).

2.6. Levodopa-induced dyskinesia rating

LID are abnormal involuntary movement (AIM) side-effects of levodopa therapy (e.g., (Bastide et al., 2015)). In the current studies we have used the well-validated rat model of LID as our primary indicator of graft function because this complex behavioral malady can be ameliorated by DA neuron grafts in parkinsonian rats (Soderstrom et al., 2008; Lane et al., 2006; Maries et al., 2006; Soderstrom et al., 2010; Lee et al., 2000) and PD patients (Hagell and Cenci, 2005). To date, all PD patients that have received a DA cell graft have been on long-term daily levodopa replacement therapy. For these reasons, behavioral assessment of LID was the primary behavioral endpoint used in our recent study demonstrating discordance between DA graft survival and behavioral efficacy in aged parkinsonian rats (Collier et al., 2015).

In the current study, LID were evaluated on pre-graft days 1, 6, 12, 20, and 25, and at five post-graft timepoints (weeks 3, 5, 6, 8, and 9 post-engraftment). AIMs induced by levodopa were rated according to a LID severity rating scale for rats developed in our laboratory based on specific criteria reflective of the nature and occurrence of multiple behavioral attributes of dyskinesia as previously detailed (e.g., (Maries et al., 2006; Steece-Collier et al., 2003; Steece-Collier et al., 2019)). On behavioral rating days, food and water were removed from the home cage to prevent interference or distractions from these sources during behavior evaluation. LID behavior was evaluated in one-minute intervals at 20, 70, 120, 170, and 220 minutes following s.c. levodopa/benserazide (12 mg/kg, 1:1). All rats were rated by the same blinded investigator throughout the duration of the study.

2.7. Preparation of donor tissue

VM tissue containing developing A8–A10 DA cell groups was dissected from wild-type (Val68Val) embryonic day 14 (E14) Sprague-Dawley dams. The VM tissue was collected in

cold calcium-magnesium free (CMF) buffer, then immediately dissociated into a homogenous cell suspension, as described previously (Collier et al., 2015). Briefly, dissected tissue was incubated in CMF buffer containing 0.125% trypsin in a bead warmer set to 37°C for 10 min. Next, the cells were triturated in 0.005% DNase using a Pasteur pipette of 2.0 mm tip diameter, followed by a sterile 3cc 22-gauge syringe. The resulting suspension was carefully layered into a conical tube containing 5 ml sterile fetal bovine serum, then pelleted by centrifugation at $190 \times g$ for 10 min at 4°C. The pellet was resuspended in 1.0 ml of Neurobasal™ medium (Gibco®; Thermo Fisher Scientific, Waltham, MA, USA). The trypan blue exclusion test was used to estimate cell number and viability. Final suspensions were prepared at a density of 33,333 cells/ μ l. Cells were kept on wet ice during transplantation surgery and used within 4 h of preparation. Cell-free Neurobasal™ medium was used for sham grafts.

2.8. Cell transplantation

After 5 weeks of levodopa priming, rats were assigned to DA graft or sham graft groups such that the mean pre-graft LID severity scores were statistically similar between groups. Rats designated to the DA graft group received an intrastriatal transplantation of 200,000 VM cells from E14 timed pregnant wild-type donors. This number of cells is known to result in robust behavioral improvement in amphetamine rotational asymmetry and amelioration of LID severity in young, wild-type parkinsonian rats (Collier et al., 2015; Maries et al., 2006). Cells were deposited at a single rostral-caudal striatal site (0.2 mm anterior, 3.0 mm lateral, relative to bregma), distributed along three dorsal-ventral coordinates at this site corresponding to 5.7, 5.0, and 4.3 mm ventral to the bottom edge of the skull (Collier et al., 2015). Each dorsal-ventral coordinate was injected with 2 μ l (0.5 μ l/min) of the VM cell suspension for a total volume of 6 μ l. Sham grafted rats received a total of 6 μ l of cell-free vehicle using the same stereotaxic coordinates. The needle was left in place for 4 min following the last injection of cells or cell-free media before being retracted. Levodopa treatment was discontinued for 1 week post-grafting to prevent any potential toxic interaction of the drug with grafted cells (Collier et al., 2015), after which levodopa treatment was reinitiated.

2.9. Graft-induced dyskinetic behavior

To provide a comprehensive assessment of GID behavior, which is an indicator of graft *dysfunction* in both PD patients and parkinsonian animal models, we employed two previously established approaches for modeling this malady: levodopa- and amphetamine-mediated GID. In rats, levodopa-mediated GID behaviors, similar to GID in PD patients, are novel (not present prior to grafting) and focal (generally localized as orolingual and forelimb stereotypy) dyskinetic behaviors that develop with graft maturation as detailed previously (Soderstrom et al., 2008; Maries et al., 2006; Soderstrom et al., 2010; Steece-Collier et al., 2003).

The alternative approach of amphetamine-mediated GID capitalizes on the finding that DA grafted, but *not* sham grafted, rats display dyskinetic behavior in response to low-dose amphetamine, which appears phenotypically similar in appearance to LID (Lane et al., 2009a; Lane et al., 2009b; Shin et al., 2012a; Smith et al., 2012a; Smith et al., 2012b). To

assess amphetamine-induced GID, rats received a single dose of amphetamine sulfate (2 mg/kg, i.p.) and were then returned to the home cage for behavioral assessment. The resulting dyskinetic behavior was evaluated by a blinded investigator using the same method and rating scale described above for LID rating.

Both levodopa- and amphetamine-mediated GID were examined after the final week 9 post-grafting LID assessment (i.e., week 10 post-grafting), with amphetamine-mediated GID rated 24 hours after levodopa-mediated GID, and approximately 24 hours prior to sacrifice to allow relevant comparisons of these two behavioral readouts and the neurochemical endpoints to which they were compared.

2.10. Necropsy

Rats were deeply anesthetized with phenytoin/pentobarbital euthanasia solution (250 mg/kg pentobarbital, i.p.; VetOne, Boise, ID, USA) then perfused intracardially with 200 ml room temperature heparinized 0.9% saline followed by 200 ml cold 4% paraformaldehyde in 0.1 M phosphate buffer. Brains were removed and post-fixed in 4% paraformaldehyde for 24 hours at 4°C, submersed in 30% sucrose solution, then stored at 4°C until time of sectioning. Brains were sectioned coronally at 40- μ m thickness using a sliding microtome and stored in a cryoprotectant solution at -20°C. Ear clippings were collected during necropsy and stored at -80°C for automated genotype confirmation (Transnetyx Inc., Cordova, TN, USA).

2.11. Histology

2.11.1. Tyrosine Hydroxylase (TH) immunohistochemistry—A 1:6 series of 40- μ m sections through the rostrocaudal extent of the brain was used for TH immunolabeling. All steps were performed at room temperature. Sections were rinsed thoroughly in tris-buffered saline containing 0.3% Triton X-100 (TBS-Tx) before incubating in 0.3% hydrogen peroxide for 15 min, then blocking in 10% normal goat serum (NGS) for 90 min. The sections were then incubated with rabbit anti-TH primary antibody (Table 1) for 24 hours. The next day, sections were incubated with biotinylated goat anti-rabbit secondary antibody with 1% NGS (Vector Laboratories, Inc., Burlingame, CA, USA; Cat No. BA-1000) for 90 min, then developed with avidin/biotin enzyme complex (Vector Laboratories, Inc., Burlingame, CA, USA; Cat No. PK6100) and 3,3'-diaminobenzidine (DAB; 0.5 mg/ml).

2.11.2. Stereological quantification of graft cell number & graft volume—A blinded investigator quantified TH-immunoreactive (THir) cells in the grafted striatum using the Stereo Investigator® Optical Fractionator workflow for total enumeration estimation (MBF Bioscience, Williston, VT, USA), similar to what we have previously reported (Collier et al., 2015). Briefly, THir cells were systematically counted within a 200 μ m \times 200 μ m counting frame superimposed on a 200 μ m \times 200 μ m grid using a 20x oil immersion objective (numerical aperture 0.75) on a Nikon Eclipse 80i microscope. This was completed in 5–7 serial (1:6) TH-immunolabeled sections throughout the striatum. The optical disector height was 22 μ m, with guard zones of 2.5 μ m.

The same sections used for graft cell counts were used for quantification of graft volume. Graft volumes were estimated using the Cavalieri Estimator probe from Stereo

Investigator®. Contours were traced around the central portion of the graft containing THir cell bodies (Fig. 4e, central black oval) in serial tissue sections by a blinded investigator. The Cavalieri probe was applied, superimposing a grid of randomly placed sampling sites (50- μm spacing) over the contours. Graft volume data are expressed as total estimated volume corrected for over-projection (mm^3).

2.11.3. Stereological quantification of neurite outgrowth—Graft-derived innervation of the host striatum was measured stereologically via the Stereo Investigator® Spaceballs workflow. For each animal, the TH-immunolabeled tissue section containing the largest portion of the graft was chosen for analysis. Rectangular contours measuring $345 \mu\text{m} \times 265 \mu\text{m}$ were drawn around regions of interest both proximal and distal to the graft, in all directions relative to the graft (i.e., medial, dorsal, lateral, ventral to the graft), for a total of eight contours. The “proximal” region was defined as a distance of 100–500 μm from the edge of the graft, with 0–100 μm from the graft serving as a “buffer zone.” Similarly, the “distal” zone was defined as 700–1100 μm from the edge of the graft, with 500–700 μm serving as an additional “middle buffer” zone. The Spaceballs workflow was applied to the contours, using systematic random sampling of sites within a grid superimposed over the contours. The probe was spherical with a radius of 5.0 μm and guard zones of 1.0 μm . Additional sites were sampled in the intact striatum using two contours of the same dimensions described above. All neurite density measurements were collected by a blinded investigator using the 60x oil immersion objective (numerical aperture 1.40) on a Nikon Eclipse 80i microscope. Data are expressed as estimated neurite length per probe volume ($\mu\text{m}/\text{mm}^3$).

2.11.4. Brightfield In Situ Hybridization (ISH)—To examine the impact of rs6265 on host striatal mRNA for the BDNF receptor, tyrosine receptor kinase B (TrkB), we performed *in situ* hybridization (ISH) for *Trkb* mRNA on 1–2 tissue sections per animal at 40- μm thickness using the manual RNAscope® 2.5 HD assay (Advanced Cell Diagnostics Inc., Hayward, CA, USA) according to manufacturer instructions, then counterstained with cresyl violet. Images (2880×2048) were acquired in the dorsolateral striatum adjacent to the graft using the 20x objective on a Nikon Eclipse Ni microscope, maintaining identical light settings across all images. The images were imported into the image visualization and analysis software, Imaris® (v. 9.3.1, Oxford Instruments) using the ImageJ (FIJI) extension. The Imaris® spots function was used to reconstruct *Trkb* mRNA puncta in a two-dimensional field of view, using the same parameters for all images, and the resulting data were exported. Data are represented as the average of values collected from two to four images per striatal hemisphere.

2.12. Immunofluorescence (IF)

In each IF assay that was performed, 1–2 representative tissue sections were used per animal. Full series tissue sections containing DAB-developed TH as described above were used as guides when choosing striatal tissue sections for IF studies, as we endeavored to select sections that contained a central portion of the DA graft in each grafted animal. To fluorescently label mRNA targets¹ (Table 2), the manual RNAscope® Multiplex Fluorescent V2 assay was used with Opal dyes (Akoya Biosciences, Marlborough, MA, USA) according

to manufacturer instructions. Following RNAscope®, IF staining for TH protein was completed using the Alexa Fluor™ 488 Tyramide SuperBoost™ Kit (goat anti-mouse IgG; Invitrogen®; Thermo Fisher Scientific, Waltham, MA, USA) according to manufacturer instructions to enhance TH fluorescence and produce bright, distinct THir fibers.

For protein-only IF assays (no mRNA), Alexa Fluor™ 488 Tyramide SuperBoost™ Kits (goat anti-rabbit IgG and goat anti-mouse IgG) were used first with TH primary antibodies pertinent to each assay (Table 1). Additional target antigens were labeled as follows after completion of the enhancement step. Briefly, TH-enhanced tissue was rinsed in TBS-Tx, then blocked in 10% serum for 1 hour at room temperature. Next, the tissue was incubated with primary antibodies pertinent to each assay (Table 1) for 24 hours at room temperature (except for synaptopodin (SP), which was incubated for 48 hours at 4°C). The tissue was then incubated with the corresponding Alexa Fluor® secondary antibodies (1:400 dilution; Table 1) for 90 min at room temperature in the dark, then mounted onto 2% subbed slides and coverslipped with Vecta-shield® anti-fade mounting medium (Vector Laboratories Inc., Burlingame, CA, USA).

2.13. Fluorescent image acquisition

Confocal images (1024 × 1024) were acquired on a Nikon A1 laser scanning confocal system equipped with a Nikon Eclipse Ti microscope and Nikon NIS-Elements AR software (v. 5.02). For synaptic characterization experiments, z-stacks were acquired through the entire thickness of the mounted tissue sections using the 60x oil-immersion objective (numerical aperture 1.40) with a digital zoom of 1.67x for a final magnification of 100x. A z-step of 0.3 μm was used per (Belmer et al., 2017) with a scan speed of 1/8 frame/sec. In the synaptic characterization analyses using TH, postsynaptic density protein 95 (PSD95), and vesicular glutamate transporters 1 and 2 (VGLUT1 and VGLUT2) described below, two images (125 μm × 125 μm) were collected in the striatum proximal to the lateral edge of the graft. The “proximal” region was defined as described above. In the TH-SP analysis, two images were collected using these same parameters, except one image was acquired in the “proximal” zone while the second image was acquired in the “distal” zone lateral to the graft border, as described above. In all experiments, additional images were collected in the intact contralateral striatum using the same parameters. Images of intact striatum were captured in striatal regions comparable to those of images collected in the grafted striatum.

For general mRNA detection and cell counts, z-stacks of the entire graft region were acquired using a 10x or 20x objective (numerical aperture 0.45 or 0.75, respectively), with a z-step of 2 μm and a scan speed of 1/8 frame/sec. In most cases, multiple images were collected in order to capture the entire graft region present in the striatal tissue section.

¹With regard to *Bdnf* mRNA, the *Bdnf* gene is transcribed into a variety of mRNA transcripts containing different 5' untranslated regions that regulate regional, stimulus-specific, and cell type-specific expression of the final protein product encoded by a single protein coding exon (Aid et al., 2007; Zuccato and Cattaneo, 2007). Accordingly, to simplify *Bdnf* mRNA detection, the ISH probe used in the current study was designed to target only the protein coding sequence (RNAscope® Probe Rn-Bdnf-CDS, Cat No. 409031).

2.14. Imaris® fluorescent image quantification

2.14.1. Dual-label protein analysis: TH and SP—Three-dimensional (3D) z-stacks of tissue immunolabeled for TH and SP proteins were imported into Imaris® and converted into native Imaris® file format. The surface function was used with semi-automatic thresholding to create an accurate 3D reconstruction of TH fibers within each image. Then, the spots function was used to reconstruct SP puncta, using the same parameters across all images. The MATLAB® “Find Spots Close to Surface” Imaris® XT plugin was then applied to the TH surface, setting the distance of putative TH-SP synapses to 0.6 μm per (Belmer et al., 2017). Data are represented as the number of SP puncta located 0.6 μm from TH fibers and normalized to TH surface volume (μm^3).

2.14.2. Dual-label protein & mRNA Analysis: TH protein and Vglut2 mRNA—Z-stacks of tissue labeled for TH protein and *Vglut2* mRNA were imported into Imaris® and a TH surface was created manually using the marching cubes function so that all THir cell bodies were accurately reconstructed with a 3D surface object. Next, the spots function was used to reconstruct *Vglut2* mRNA puncta, using the same parameters across all images. A binary mask was applied to the TH surface. The *Vglut2* mRNA spots were then filtered using the masked channel so that only *Vglut2* mRNA puncta inside TH surface objects were included in the analysis. Finally, the MATLAB® “Split into Surface Objects” plugin was applied to the filtered spots and the resulting data were exported. In cases where multiple images were acquired to include the entire graft region, the data are expressed as the sum of the values from all images collected per animal. Care was taken to ensure that the same cells were not counted twice in adjacent images. Only THir cells with 2 *Vglut2* mRNA puncta were included for analysis.

2.14.3. Triple-label protein analysis: TH, VGLUT2, & PSD95 proteins—Z-stacks of tissue immunolabeled for TH and VGLUT2 (presynaptic markers) combined with PSD95 (postsynaptic marker) were imported into Imaris®. The surface function was used with semi-automatic thresholding to create accurate 3D reconstructions of TH fibers and PSD95. The spots function was applied to reconstruct VGLUT2 protein puncta within each image, using the same parameters across all images. Next, a binary mask was applied to the TH surface object. PSD95 surfaces were filtered using the masked channel to obtain PSD95 surfaces located outside of the TH surface (PSD95(out)). Similarly, VGLUT2 spots were filtered using the masked channel to select VGLUT2 spots with centers located inside the TH surface (VGLUT2(in)). Then, the MATLAB® “Find Spots Close to Surface” plugin was used to find VGLUT2(in) 0.6 μm from PSD95(out). Finally, the MATLAB® “Distance Transformation” plugin was used to find PSD95(out) surfaces located 0.6 μm from the TH surface. Data are represented as the number of VGLUT2 (in) puncta, number of VGLUT2(in)-PSD95(out) appositions, and total volume of PSD95(out) surfaces, all normalized to TH surface volume (μm^3).

2.14.4. Triple-label protein analysis: TH, VGLUT1, & PSD95 proteins—Z-stacks of tissue immunolabeled for TH, VGLUT1, and PSD95 proteins were imported into Imaris® and deconvolved using Imaris Clear-View™ Deconvolution to improve image clarity (iterative algorithm with 10 iterations, pinhole = 15.3 μm , specimen refractive index = 1.37,

distance from coverslip = 7.97 μm). Next, 3D surface objects of TH and PSD95 were created using semi-automatic thresholding, as described above. The spots function was used to create VGLUT1 protein puncta, maintaining the same parameters across all images. As before, a binary mask was applied to the TH surface object, and VGLUT1 spots were filtered using the masked channel to find VGLUT1 puncta located outside of the TH surface (VGLUT1(out)). Similarly, the PSD95 surface objects were filtered by the masked channel to find PSD95 structures located inside the TH surface (PSD95(in)). Then, the MATLAB® “Find Spots Close to Surface” plugin was used to find VGLUT1(out) located 0.6 μm from the TH surface and VGLUT1(out) located 0.6 μm from PSD95(in). Data are represented as the number of VGLUT1(out) puncta near (0.6 μm) the TH surface and the number of VGLUT1(out)-PSD95 (in) appositions, all normalized to TH surface volume (μm^3).

2.14.5. Dual-label protein & mRNA analysis: TH protein & tryptophan hydroxylase 2 (Tph2) mRNA—Z-stacks of tissue labeled for TH protein and *tryptophan hydroxylase 2 (Tph2)* mRNA (i.e., an isozyme of tryptophan hydroxylase, the rate-limiting enzyme in the synthesis of serotonin (5-hydroxytryptamine (5-HT) and marker for 5-HT neurons) were imported into Imaris®. Surface objects for TH protein and *Tph2* mRNA (which presented as a soma-filling, rather than punctate, stain) were created manually with the marching cubes function so that all cell bodies containing *Tph2* mRNA or TH protein were accurately reconstructed in 3D. The number of surface objects for each cell type was recorded. Because of limited amount of striatal tissue containing grafted neurons and extensive analyses done in our study, data are expressed as the number of *Tph2* mRNA-containing cells (i.e., 5-HT neurons) relative to the number of THir cells (i.e., DA neurons) in each image (*Tph2*/TH ratio) in 2 striatal sections. Care was taken to ensure that the same grafted cells were not counted twice in adjacent images.

2.14.6. Dual-label protein & mRNA analysis: TH protein & Bdnf mRNA—Because of limited amount of striatal tissue containing grafted neurons and the extensive analyses done in our study, tissue from only 3 Val68Val subjects was available for examining *Bdnf* mRNA in grafted DA neurons, while grafted tissue from 9 Met68Met subjects was available for this assay. Z-stacks of tissue immunolabeled for TH protein and *Bdnf* mRNA were imported into Imaris®. Surface objects for TH were created manually with the marching cubes function so that all THir cells were accurately reconstructed in 3D. Next, the spots function was used to reconstruct *Bdnf* mRNA puncta, using the same parameters across all images. The MATLAB® “Split into Surface Objects” plugin was applied to the *Bdnf* mRNA spots and the resulting data were exported. As described above, in cases where multiple images were acquired to include the entire graft region, the data are expressed as the sum of the values from all images collected per animal. Care was taken to ensure that the same grafted cells were not counted twice in adjacent images. Only THir cells with 2 *Bdnf* mRNA puncta were included for analysis.

2.15. BDNF release and tissue content in rs6265 rats

2.15.1. BDNF release in hippocampal cultures—Timed pregnant (embryonic day 18) female Val68Val or Met68Met rats were deeply anesthetized with pentobarbital (50 mg/kg, i.p.). Hippocampi were dissected using a Leica dissecting microscope and pooled in

cold, sterile, CMF buffer (pH 7.3). Cell suspensions were prepared through a series of CMF rinses, incubation in 0.125% trypsin for 10 minutes at 37°C, rinsing in CMF again, and trituration in 0.004% DNase to disperse the cells into solution. Trypan blue was used to assess cell viability. Cell suspensions of 95% viability were plated at a density of 1,000,000 cells/well on poly-D-lysine coated 6-well plates in Neurobasal™ medium supplemented with B27.

For determining basal BDNF release, 72 hours after plating, all culture media was removed and replaced with artificial cerebrospinal fluid (aCSF: 125 mM NaCl, 2.5 mM KCl, 1.25 mM NaH₂PO₄, 25 mM NaHCO₃, 2 mM CaCl₂, 1 mM MgCl₂, 25 mM glucose). Thirty minutes later aCSF was collected for analysis of BDNF via ELISA as per manufacturer's instructions (BDNF Emax ELISA, Promega, Madison, WI) using samples loaded in triplicate.

2.15.2. BDNF tissue content in rs6265 rats—For determination of BDNF tissue content, tissue punches from the hippocampus, striatum, and M1 cortex were collected from 3-month-old male Val68Val, Val68Met, and Met68Met rats. Samples were thawed on ice and 250 µl of RIPA Lysis Buffer System was added to each sample (sc-249–48, Santa Cruz Biotechnology, Dallas, TX). Samples were homogenized by sonication on ice, followed by a 30-minute incubation after which a portion of the sample was taken for total protein determination via Pierce BCA Assay (ThermoFischer, Waltham, MA) per manufacturer's instructions. The remaining sample was centrifuged and the supernatant collected. A BDNF ELISA was completed on triplicate samples as per manufacturer's instructions. BDNF levels in tissue lysates (picogram (pg)) were calculated per milligram (mg) total protein.

2.16. Statistical Analysis

All LID and GID behavioral data were analyzed by non-parametric statistics including Kruskal-Wallis with Dunn's multiple comparison tests or Mann-Whitney *U* tests (between subject comparisons) and Friedman tests with Dunn's multiple comparison tests (within subjects comparisons). Amphetamine rotations were analyzed using an unpaired two-tailed *t*-test with Welch's correction to account for unequal variances and one-way ANOVA with Šídák's multiple comparisons test.

Unpaired two-tailed *t*-tests were used to compare the following data between genotypes: grafted DA neuron cell counts, graft volumes, 5-HT/DA neuron ratios, *Vglut2* mRNA expression in naïve SNc and ventral tegmental area (VTA) separately, and DA neuron *Bdnf* mRNA expression (expressed as percentage of total DA neurons). Unpaired one-tailed *t*-tests were used to compare neurite outgrowth in each direction (dorsal, ventral, medial, lateral) surrounding the DA graft between genotypes. An unpaired two-tailed *t*-test with Welch's correction was used to analyze the level of *Bdnf* transcript in grafted DA neurons.

Two-way ANOVAs were used to compare *Vglut2* mRNA expression between naïve and grafted animals of both genotypes (2 × 2: genotype × treatment) and VGLUT2 protein content in DA neuron fibers (2 × 3: genotype × treatment), combined with Šídák's multiple comparisons test and Tukey's multiple comparisons test, respectively. Two-way repeated measures ANOVAs were used with Šídák's multiple comparisons test to analyze the

following data: grafted neurite outgrowth (2×2 : genotype \times distance from graft), neurite density vs intact contralateral striatum (2×2 : genotype \times treatment), proximal and distal TH-SP contact densities within each genotype (2×2 : genotype \times distance from graft), PSD95 volume near DA fibers (2×2 : genotype \times treatment), VGLUT1-PSD95 appositions (2×2 : genotype \times treatment), VGLUT1 input onto DA neurons (2×2 : genotype \times treatment), total VGLUT1 innervation (2×2 : genotype \times treatment), and *Trkb* mRNA expression in host striatum (2×2 : genotype \times treatment).

A one-way mixed-effects model with repeated measures was used with the post-hoc Holm-Šídák's multiple comparisons test to analyze distal neurite density separated by region for each genotype. TH-SP contact density comparisons between lesioned and intact striatum, and between genotypes, were analyzed using a two-way mixed-effects model with repeated measures and Šídák's and Dunnett's multiple comparisons tests (2×3 : genotype \times treatment). VGLUT2(in)-PSD95 (out) apposition data were analyzed using a two-way mixed-effects model with repeated measures (2×2 : genotype \times treatment) and Šídák's multiple comparisons test.

Non-parametric Spearman correlation tests were used for all correlations with LID and GID behavior. Correlations with amphetamine rotational behavior were analyzed using Pearson correlation. Statistical outliers, though uncommon, were identified using ROUT and Grubbs' outlier tests. Parametric statistical tests were chosen for analysis only when data met assumptions for normality and homogeneity of variances. All statistical analyses were completed using GraphPad Prism® software for Windows (v. 8.4.2).

3. RESULTS

3.1. Impact of the Met allele on behavioral measures of DA graft function

3.1.1. Met68Met rats show enhanced behavioral efficacy compared to wild-type Val68Val rats—We hypothesized that as a consequence of reduced BDNF release in Met68Met rats, these subjects would experience reduced graft-mediated improvement of LID. In contrast to this hypothesis, Met68Met rats showed enhanced functional benefit from VM DA grafts compared to wild-type subjects as indicated by a more rapid and overall greater decrease in LID severity. Specifically, parkinsonian DA grafted Met68Met rats showed a significant reduction in LID severity compared to DA grafted Val68Val and sham grafted subjects beginning 5 weeks post-grafting (Fig. 2a; Week 5: $p = 0.0015$ Met68Met-DA vs Sham, $p = 0.0302$ Met68Met-DA vs Val68Val-DA; Week 6: $p = 0.0284$ Met68Met-DA vs Sham, $p = 0.0475$ Met68Met-DA vs Val68Val-DA; Week 8: $p = 0.0198$ Met68Met-DA vs Sham; Week 9: $p = 0.0003$ Met68Met-DA vs Sham). In contrast, the DA grafted Val68Val rats required 8 weeks to display a similar level of reduction in LID severity; however, a statistically meaningful reduction was not apparent until 9 weeks post-engraftment (Fig. 2a,c; $p = 0.0312$ Val68Val DA graft; $p = 0.0078$ Met68Met DA graft; $p = 0.0078$ sham graft; vs pre-graft baseline, Wilcoxon matched-pairs signed rank test). At the final 9 week post-graft timepoint, the DA grafted Met68Met rats showed a $73.92 \pm 12.51\%$ (mean \pm SEM) reduction and the DA grafted Val68Val rats a $55.21 \pm 2.22\%$ reduction in total LID severity (Fig. 2a,c).

While it has been reported that PD patients with the Met allele show a significantly higher risk of developing LID earlier in the time course of treatment (Foltynie et al., 2009), to the best of our knowledge no information is available on whether this results in enhanced severity over time. In contrast to this clinical report, we found no significant impact of genotype on LID in the sham grafted rats using high dose levodopa (Kruskal-Wallis, $p = 0.12$ for all time points post-engraftment). Accordingly, for the post-graft time period, the sham groups were combined.

Evidence of enhanced benefit in DA grafted Met68Met compared to Val68Val rats was also observed using amphetamine-induced rotational asymmetry examined at 7 weeks post-engraftment (one-way ANOVA with Šídák's post-hoc test, $p = 0.0301$; Fig. 2diii).

Interestingly, while there was a difference in pre-graft amphetamine rotational rate with Met68Met rats showing significantly fewer rotations per minute than Val68Val rats (Fig. 2dii; $p = 0.0023$, Val68Val vs Met68Met, Unpaired t -test with Welch's correction), there was no significant difference between genotypes in the sham grafted rats at the 7 week post-graft timepoint (Fig. 2diii; $p = 0.5620$, Val68Val vs Met68Met; two-way ANOVA with Šídák's multiple comparisons test). Of note was the homogeneity of response to amphetamine, both pre- and post-graft, in Met68Met subjects (Fig. 2dii, iii).

3.2. Impact of the Met allele on behavioral measures of DA graft dysfunction

3.2.1. The Met allele is associated with the development of GID in response to levodopa and amphetamine—In keeping with our hypothesis that Met68Met rats would experience elevated graft-derived side-effects, GID behavior was manifest only in Met68Met rats under the current grafting protocol which resulted in wide-spread striatal reinnervation (Maries et al., 2006) (Fig. 3a–d). There was a single Val68Val DA grafted rat that displayed a low level of amphetamine-mediated GID and a moderate level of levodopa-mediated GID. While both of these behaviors have been reported to be uniquely associated with DA grafting in parkinsonian rats (Soderstrom et al., 2008; Maries et al., 2006; Soderstrom et al., 2010; Steece-Collier et al., 2003; Lane et al., 2009a; Lane et al., 2009b; Shin et al., 2012a; Smith et al., 2012a; Smith et al., 2012b), we provide here the first direct comparison of these behavioral assays. While both methods of GID assessment support that the Met risk allele is associated with induction of aberrant GID-like behaviors, based on differences in their phenotype (see “Graft-Induced Dyskinetic Behavior” section above) it is not necessarily surprising that there is a lack of correlation of these behaviors with each other (Fig. 3e). Future investigations may be warranted for understanding mechanistic differences between amphetamine- and levodopa-mediated GID behaviors in this rat model of neural grafting.

3.3. Impact of the Met allele on graft survival and neurite outgrowth

3.3.1. Despite equal numbers of surviving grafted DA neurons, graft-derived reinnervation is more extensive in Met68Met than in Val68Val striatum—Large, TH⁺ grafts of DA neurons were observed in all VM grafted subjects, extending neurites into the surrounding striatal parenchyma (Fig. 4a). TH-immunoreactivity in the lesioned striatum is presumed to be derived from grafted DA neurons based on the fact that there was a near-complete depletion of host nigral DA neurons in animals of both genotypes. The mean

percent lesion was similar between genotypes (mean percent SNc DA neuron loss compared to intact hemisphere \pm SEM: Val68Val: $96.31 \pm 0.60\%$ depletion with a range of 92.5–98.5%; Met68Met: $96.59 \pm 0.32\%$ depletion with a range of 94.00–99.4%; Fig. 4b and Supplementary Fig. 3). Stereological quantification indicated that the number of surviving transplanted DA neurons was not different between genotypes (mean estimated total number of grafted DA neurons \pm SEM: Val68Val: 2922.63 ± 694.46 ; Met68Met: 2978.86 ± 592.43 ; $t(11) = 0.0604$, $p = 0.9529$, Fig. 4c). Accordingly, graft volumes also did not differ significantly (mean volume \pm SEM: Val68Val: $0.5835 \pm 0.1254 \text{ mm}^3$; Met68Met: $0.5394 \pm 0.0940 \text{ mm}^3$; $t(11) = 0.2858$, $p = 0.7803$; Fig. 4d).

In contrast to what would be expected in an environment of reduced activity-dependent BDNF release, but in keeping with the functional evidence described above, stereological quantification (Fig. 4e) demonstrated that neurite outgrowth was significantly more extensive in Met68Met than in Val68Val subjects (Fig. 4a, higher magnification images). While both genotypes exhibited similarly robust neurite density proximal to the graft (Fig. 4f), there was a significant impact of the Met68Met genotype on graft-derived neurite outgrowth observed at regions distal to the graft (Fig. 4a,f; mean distal neurite density \pm SEM: Val68Val: $0.3189 \pm 0.0363 \mu\text{m}/\text{mm}^3$; Met68Met: $0.4655 \pm 0.0303 \mu\text{m}/\text{mm}^3$; two-way repeated measures ANOVA $F(1,11) = 5.958$, $p = 0.0328$; Šídák's multiple comparisons test: Proximal: $t(22) = 2.011$, $p = 0.1103$; Distal: $t(22) = 2.424$, $p = 0.0475$). Notably, in Met68Met subjects, the more robust distal neurite outgrowth was evenly distributed in all regions surrounding the graft (i.e., dorsal, ventral, lateral, medial; mixed-effects model $F(1.168, 5.449) = 0.6657$, $p = 0.4723$; Fig. 4g). This contrasts with that observed in the striatum of Val68Val subjects, where the densest neurite growth was restricted to the dorsal striatum. While neurite density in the dorsal region of Val68Val striatum was not significantly different from other regions surrounding the graft (mixed-effects model $F(1.551, 7.756) = 1.970$, $p = 0.2037$), neurite outgrowth was significantly less in ventral and medial regions when compared to Met68Met subjects (Ventral: $t(8) = 2.244$, $p = 0.0275$; Medial: $t(9) = 2.054$, $p = 0.0351$).

In proximal regions, graft-derived reinnervation of the parkinsonian striatum was statistically similar to the intact striatum regardless of genotype (two-way repeated measures ANOVA $F(1,11) = 1.041$, $p = 0.3295$; Šídák's multiple comparisons test: Val68Val: $t(11) = 2.097$, $p = 0.1163$ vs intact; Met68Met: $t(11) = 1.007$, $p = 0.5586$ vs intact; Supplementary Fig 4). Specifically, graft-derived reinnervation proximal to the graft reached $80.98 \pm 4.05\%$ and $87.56 \pm 4.49\%$ of THir neurite density observed in the intact hemisphere for Val68Val and Met68Met rats, respectively. This was not observed distal to the graft, where THir neurite density was significantly less than that of the intact striatum for animals of both genotypes (two-way repeated measures ANOVA $F(1,11) = 73.22$, $p < 0.0001$; Šídák's multiple comparisons test: Val68Val: $t(11) = 5.650$, $p = 0.0003$ vs intact; Met68Met: $t(11) = 6.650$, $p < 0.0001$ vs intact; Fig. 4h). Indeed, graft-derived reinnervation distal to the graft reached only $35.43 \pm 5.56\%$ and $48.21 \pm 7.40\%$ of that observed in the intact hemisphere in Val68Val and Met68Met rats, respectively. Notably, though distal reinnervation was significantly less than in the intact striatum for both genotypes, the percentage of reinnervation distal to the DA graft was significantly higher in Met68Met subjects ($t(11) = 3.058$, $p = 0.0109$).

3.4. Impact of the Met allele on presumed graft connectivity with host medium spiny neurons (MSNs)

3.4.1. Presumed graft-host synaptic connections are correlated with LID behavior in Val68Val but not Met68Met rats, despite similar contact densities—

Synaptopodin/SP is an actin-associated structural protein found in mature dendritic spines (Vlachos et al., 2009; Segal et al., 2010). We used dual-label immunofluorescence (TH to label striatal DA fibers; SP to label host MSN dendritic spines) with confocal microscopy and Imaris® 3D reconstruction to quantify the number of presumed synaptic contacts formed between THir fibers and their preferential target, the dendritic spines of striatal MSNs (Fig. 5a,b) per (Collier et al., 2015).

Val68Val and Met68Met rats had similar TH-SP synaptic contact densities, both proximal (TH-SP appositions per μm^3 TH \pm SEM: Val68Val: 0.3532 ± 0.0840 ; Met68Met: 0.2731 ± 0.0230 ; mixed effects model $F(1,12) = 0.4762$, $p = 0.5033$; Šídák's multiple comparisons test: $t(4.606) = 0.9205$, $p = 0.7872$; Fig. 5c) and distal to the graft (Val68Val: 0.4596 ± 0.1093 ; Met68Met: 0.3433 ± 0.0338 ; mixed effects model $F(1,12) = 0.4762$, $p = 0.5033$; Šídák's multiple comparisons test: $t(4.784) = 1.025$, $p = 0.7308$; Fig. 5c). Moreover, the density of TH-SP appositions in the reinnervated striatum was statistically similar to that of the intact contralateral striatum, except for the proximal region in parkinsonian Met68Met striatum, which was significantly lower than that of the intact contralateral striatum (TH-SP contact density versus intact striatum; mixed-effects model $F(1.523, 16.00) = 3.649$, $p = 0.0596$; Dunnett's multiple comparisons test: Val Proximal: $q(4) = 2.464$; $p = 0.1148$; Val Distal: $q(4) = 0.0599$, $p = 0.9974$; Met Proximal: $q(6) = 3.234$, $p = 0.0313$; Met Distal: $q(6) = 1.134$, $p = 0.4642$).

As expected, TH-SP connectivity was negatively correlated with total LID severity on the final rating day in wild-type (Val68Val) rats (Fig. 5d). Specifically, Val68Val subjects with more TH-SP synaptic appositions showed a greater reduction in the severity of LID behavior, consistent with previous data from our group (Collier et al., 2015). This correlation was statistically significant for synaptic appositions located in the region with more dense reinnervation proximal to the graft (Proximal: Spearman $r = -1.00$, $p = 0.0167$; Distal: Spearman $r = -0.90$, $p = 0.0833$; Fig. 5d,e). Surprisingly, there were no significant correlations of these appositions with total LID severity in Met68Met rats (Proximal: Spearman $r = -0.50$, $p = 0.2162$; Distal: Spearman $r = -0.0714$, $p = 0.8820$). Additionally, TH-SP synaptic contact density did not correlate with amphetamine-mediated GID, levodopa-mediated GID, or post-graft amphetamine-induced rotational behavior for either genotype (data not shown).

3.5. Atypical glutamatergic phenotype in grafted dopamine neurons

3.5.1. Grafted DA neurons maintain an immature phenotype, as evidenced by elevated Vglut2 mRNA and corresponding protein expression compared to the naïve adult midbrain—

Preclinical electron microscopic data from rat studies in our lab (Soderstrom et al., 2008), together with evidence from grafted parkinsonian non-human primates (Leranth et al., 1998) and postmortem clinical evidence in grafted PD patients (Kordower et al., 1996), show that grafted DA neurons make asymmetric (presumed

excitatory/glutamatergic) synapses onto unlabeled dendrites and dendritic spines in the host striatum. Accordingly, we sought to characterize the expression of vesicular glutamate transporter in embryonic DA neurons transplanted into the parkinsonian striatum by quantifying levels of *Vglut2* mRNA and protein in this cell population. We demonstrate here, to the best of our knowledge, the first evidence that grafted THir neurons show colocalization with *Vglut2* mRNA (TH+/ *Vglut2*+; Fig. 6b,c). We also demonstrate that VM-derived grafts contain TH-only (TH+/ *Vglut2*-) neurons, and an abundance of centrally-located TH-/ *Vglut2*+ cells (Fig. 6b,c). Overall, in VM grafts transplanted into animals of both genotypes, we observed TH-only, *Vglut2*-only, and combined TH+/ *Vglut2*+ cells, similar to what has been observed in the naïve midbrain (Morales and Margolis, 2017; Morales and Root, 2014) (Fig. 6d).

Remarkably, nearly 60% of grafted DA neurons contained *Vglut2* mRNA in host animals of both genotypes at 10 weeks post-engraftment (percent of grafted DA neurons containing *Vglut2* mRNA: Val68Val: $57.34 \pm 5.13\%$; Met68Met: $57.96 \pm 4.34\%$), a time at which midbrain DA neurons should be fully mature (Prakash and Wurst, 2006). In contrast, we found that naïve (endogenous) midbrain DA neurons in both genotypes had significantly less *Vglut2* mRNA compared to grafted DA neurons (percent of naïve midbrain DA neurons expressing *Vglut2* mRNA: Val68Val: $12.4 \pm 1.95\%$; Met68Met: $33.13 \pm 6.42\%$; two-way ANOVA $F(1,18) = 38.00$, $p < 0.0001$; Šídák's multiple comparisons test: Val68Val: $t(18) = 4.996$, $p = 0.0002$, naïve vs grafted; Met68Met: $t(18) = 3.615$, $p = 0.0040$, naïve vs grafted; Fig. 6e).

It is noteworthy that although grafted DA neurons expressed similar levels of *Vglut2* mRNA, this was not the case when comparing endogenous DA neurons located in the naïve midbrain. Specifically, SNc and VTA DA neurons in naïve adult Met68Met midbrain expressed significantly more *Vglut2* mRNA than their wild-type counterparts (SNc: $t(7) = 3.062$, $p = 0.0183$; VTA: $t(7) = 2.524$, $p = 0.0396$; Fig. 6e).

To corroborate that grafted DA neurons maintained an immature DA/glutamate co-expression phenotype, we sought evidence of VGLUT2 protein in the grafted TH neurites. VGLUT2 protein was indeed found to be colocalized within grafted THir neurites in the grafted parkinsonian striatum (Fig. 7a). This is in contrast to the naïve brain, where there was sparse evidence of TH-VGLUT2 colocalization in the striatum (Fig. 7b). Indeed, grafted THir neurites contained significantly more VGLUT2 protein than nigrostriatal THir fibers in the naïve striatum (two-way ANOVA $F(2,32) = 14.44$, $p < 0.0001$; Tukey's multiple comparisons test, naïve vs grafted striatum: Val68Val: $q(32) = 5.497$, $p = 0.0014$; Met68Met: $q(32) = 4.897$, $p = 0.0043$; Fig. 7b). Unexpectedly, TH-VGLUT2 colocalization was also increased in the intact contralateral striatum of grafted parkinsonian rats compared to experimentally naïve animals (two-way ANOVA $F(2,32) = 14.44$, $p < 0.0001$; Tukey's multiple comparisons test, naïve vs intact striatum: Val68Val: $q(32) = 4.462$, $p = 0.0095$; Met68Met: $q(32) = 3.564$, $p = 0.0435$; Fig. 7b). The implications of this plasticity response in the intact striatum contralateral to the lesioned/grafted striatum remains to be determined, though we contend that this finding speaks to the importance of including additional controls for comparison beyond just the unlesioned hemisphere, which has historically been used as a within-subject control in this hemiparkinsonian rat model. There were no significant

differences in VGLUT2 protein content within striatal THir fibers between genotypes (Fig. 7b).

Interestingly, TH-VGLUT2 colocalization was significantly and positively correlated with amphetamine-mediated GID behavior in Met68Met subjects that displayed this aberrant graft-associated behavior (GID+ rats, i.e., total GID score >10; Spearman $r = 1.00$, $p = 0.0167$; Fig. 7c). In contrast, significant correlations were not observed in Val68Val subjects that expressed very low levels of this GID behavior (Spearman $r = 0.70$, $p = 0.2333$; Fig. 7c) or in the smaller subset of Met68Met subjects that did not display GID behavior (GID-rats, i.e., total GID score ≤ 10 ; Spearman $r = 0.80$, $p = 0.3333$). No significant correlations were found between TH-VGLUT2 colocalization and levodopa-mediated GID, LID, or post-graft amphetamine rotational behavior.

3.5.2. Grafted DA neurons show neurochemical signatures of excitatory synapses in the parkinsonian striatum—

Next, we examined whether grafted DA neurons containing VGLUT2 protein showed neurochemical evidence of atypical, presumed neurochemically active, excitatory synapses. To address this question, we used triple-label immunofluorescence for TH, VGLUT2, and PSD95, a post-synaptic scaffolding protein found in excitatory synapses and a potent regulator of synaptic strength (e.g., (Chen et al., 2011)). We define here a putative “neurochemically active” excitatory synapse as presynaptic VGLUT2 protein present *within* a THir neurite (VGLUT2(in); i.e., pre-synaptic) and in close proximity ($\leq 0.6 \mu\text{m}$) to PSD95 protein located outside of the THir fibers (PSD95(out); i.e., post-synaptic; Fig. 7d) per (Belmer et al., 2017). Similar synaptic mapping approaches involving confocal microscopy and computational software paired with electro-physiology have shown correlation of these “putative” synapses with neuronal firing output (Iascone et al., 2020). In the present study, putative excitatory synapses made by DA neurons in the grafted striatum were observed in DA grafted animals of both genotypes, though the number of excitatory synapses did not differ significantly between Val68Val and Met68Met subjects (mixed-effects model $F(1,12) = 1.737$, $p = 0.2121$; Fig. 7e). The number of VGLUT2(in)-PSD95(out) appositions, however, was increased in grafted striatum compared to the intact contralateral striatum in animals of both genotypes (mixed-effects model $F(1,10) = 28.70$, $p = 0.0003$; Šídák’s multiple comparisons test: Val68Val: $t(10) = 4.054$, $p = 0.0046$; Met68Met: $t(10) = 3.544$, $p = 0.0106$; Fig. 7e).

We have previously reported (Soderstrom et al., 2008) a positive trend between atypical THir asymmetric contacts onto host striatal cells and *levodopa*-mediated GID behavior using immunoelectron microscopy, though a statistically significant correlation was not found. In the present study, the number of THir asymmetric synaptic contacts (i.e., TH-normalized VGLUT2(in)-PSD95(out) synaptic appositions) was significantly, positively correlated with *amphetamine*-mediated GID in Met68Met subjects (Spearman $r = 0.74$, $p = 0.0458$), but not in Val68Val subjects that displayed very low levels of this behavior (Spearman $r = 0.80$, $p = 0.1333$; Fig. 7f). Furthermore, in the current study, the number of THir asymmetric contacts showed a positive trend in Met68Met rats but did not significantly correlate with *levodopa*-mediated GID, similar to (Soderstrom et al., 2008). They also did not correlate with LID or post-graft amphetamine rotational behavior (Supplementary Fig. 5).

Postsynaptically, there was significantly more PSD95 in close proximity ($< 0.6 \mu\text{m}$) to THir fibers in the grafted striatum (vs intact striatum) only in Met68Met rats, indicating an increase in asymmetric synaptic contacts made by DA neurons in the grafted striatum in Met allele carriers (two-way repeated measures ANOVA $F(1,10) = 15.72$, $p = 0.0027$; Šídák's multiple comparisons test: Val68Val: $t(10) = 2.168$, $p = 0.1077$; Met68Met: $t(10) = 3.577$, $p = 0.0100$; Supplementary Fig. 6a). This was found to be true despite similar total PSD95 volumes between intact and grafted Met68Met striatum (two-way repeated measures ANOVA $F(1,10) = 1.037$, $p = 0.3326$; Šídák's multiple comparisons test: $t(10) = 1.267$, $p = 0.4132$; Supplementary Fig. 6b).

3.6. Excitatory corticostriatal synaptic input onto grafted dopamine neurons

3.6.1. Atypical glutamatergic (VGLUT1) input onto striatal THir fibers is significantly increased in the grafted striatum only in Met68Met rats—Previous studies have identified unlabeled asymmetric synapses (presumed corticostriatal afferents) onto somas and dendrites of grafted primary DA neurons in the parkinsonian striatum (Fig. 8a; (Soderstrom et al., 2008; Kordower et al., 1996)). Importantly, previous evidence from our lab indicated that these atypical synaptic connections correlated with levodopa-mediated GID behavior in grafted parkinsonian rats (Soderstrom et al., 2008). To assess whether this phenomenon is associated with GID in -Met allele carrying subjects, we employed triple-label immunofluorescent staining for VGLUT1 (a marker for pre-synaptic corticostriatal afferents), PSD95, and TH (Fig. 8b,c) and then quantified the number of these synaptic triads (VGLUT1+PSD95+TH; Fig. 8d). Pre-synaptic VGLUT1 puncta (VGLUT1(out)) in close apposition ($< 0.6 \mu\text{m}$) to PSD95 positioned inside THir fibers (PSD95(in)), which we defined as putative excitatory synapses onto grafted DA neurons, were exceedingly rare. Though the number of VGLUT1(out)-PSD95(in) appositions appeared to increase in grafted striatum, this finding was not statistically significant for either genotype (two-way repeated measures ANOVA $F(1,10) = 5.317$, $p = 0.0438$; Šídák's multiple comparisons test: Val68Val: $t(10) = 1.346$, $p = 0.3728$; Met68Met: $t(10) = 1.980$, $p = 0.1460$; Fig. 8d) or between genotypes (two-way repeated measures ANOVA $F(1,10) = 5.341$, $p = 0.0434$; Šídák's multiple comparisons test: Grafted: $t(20) = 0.9922$, $p = 0.5551$; Intact: $t(20) = 1.419$, $p = 0.3133$; Fig. 8d). Moreover, the number of these synaptic triads did not correlate with GID, LID, or post-graft amphetamine rotational behavior (data not shown).

While these excitatory neurochemical triads were rare, there was, as expected, an abundance of VGLUT1 protein (indicating corticostriatal afferents) in the intact and grafted striatum. There also was a relative abundance of VGLUT1 making apparent appositions onto THir fibers, defined as VGLUT1 puncta located $> 0.6 \mu\text{m}$ from THir fibers (Belmer et al., 2017) in both the intact and grafted striatum. While there was no difference in the total amount of VGLUT1 in the striatum between genotypes or between intact and grafted striata (two-way repeated measures ANOVA $F(1,10) = 2.862$, $p = 0.1215$), we did find that the VGLUT1 corticostriatal afferents showed increased apposition onto TH fibers in grafted striatum (vs intact striatum) in Met68Met but not Val69Val rats (two-way repeated measures ANOVA $F(1,10) = 8.929$, $p = 0.0136$; Šídák's multiple comparisons test: Val68Val: $t(10) = 0.1938$, $p = 0.9776$; Met68Met: $t(10) = 4.858$, $p = 0.0013$; Fig. 8e).

While DA grafted Met68Met rats (a group displaying significant GID behavior) were found to have significantly higher levels of corticostriatal VGLUT1-TH appositions in grafted compared to the intact striatum, statistical correlations were not found between these appositions and amphetamine-mediated GID, levodopa-mediated GID, or post-graft amphetamine rotational behavior for either genotype.

3.7. Impact of the Met allele on presence of 5-HT neurons in VM grafts

3.7.1. VM grafts contain modestly, but significantly more 5-HT neurons when transplanted into Met68Met striatum—Serotonergic neurons (i.e., cells containing *Tph2* mRNA) were observed in VM grafts in host subjects of both genotypes (Fig. 9a). However, these grafts in Met68Met hosts contained a modest but significantly higher proportion of 5-HT neurons relative to the number of transplanted DA neurons (expressed here as the 5-HT/DA cell ratio) compared to Val68Val hosts (mean 5-HT/DA cell ratio \pm SEM: Val68Val: 0.2559 ± 0.0262 ; Met68Met: 0.355 ± 0.0274 ; $t(12) = 2.378$, $p = 0.0349$; Fig. 9b).

3.7.2. 5-HT neurons in VM grafts are not associated with amphetamine-mediated or levodopa-mediated GID behavior—The presence of 5-HT neurons in VM grafts transplanted into parkinsonian striatum was not associated with GID behavior in the current study. Specifically, there was no correlation between the 5-HT/DA cell ratio and amphetamine-mediated GID (Val68Val: Spearman $r = 0.60$, $p = 0.3500$; Met68Met: Spearman $r = -0.18$, $p = 0.6436$; Fig. 9c) or levodopa-mediated GID (Val68Val: Spearman $r = 0.67$, $p = 0.2667$; Met68Met: Spearman $r = -0.29$, $p = 0.4421$; Fig. 9d). Furthermore, we found no significant correlation between the 5-HT/DA cell ratio and LID severity, though both groups exhibited moderately strong correlations in *opposite directions* (i.e., increasing 5-HT/DA ratio, increasing LID severity in Val68Val rats; increasing 5-HT/DA ratio, decreasing LID severity in Met68Met rats) (Val68Val: Spearman $r = 0.70$, $p = 0.2333$; Met68Met: Spearman $r = -0.53$, $p = 0.1475$; Fig. 9e). There also was no correlation between post-graft amphetamine rotational behavior and the 5-HT/DA cell ratio in VM grafts for either genotype (data not shown).

3.8. Impact of the Met allele on Bdnf mRNA expression in grafted DA neurons and Trkb mRNA expression in host striatum

3.8.1. Bdnf mRNA is abundant in DA grafts transplanted into both Val68Val and Met68Met hosts—As the present study emphasizes a shift in focus to the environment into which embryonic cells are transplanted, we sought to characterize the effects of host genotype on expression of *Bdnf* mRNA within wild-type grafted DA neurons. Under normal conditions, *Bdnf* mRNA is rarely observed in the striatum (e.g., (Altar et al., 1997; Altar and DiStefano, 1998; Baydyuk and Xu, 2014)). Instead, BDNF protein is anterogradely transported to the striatum primarily from the motor cortex and SNc DA neurons (Altar et al., 1997). As such, grafted DA neurons may be an important source of BDNF to the denervated, parkinsonian striatum (Fig. 10a). Thus, we examined whether the disparate levels of extracellular host striatal BDNF in Met68Met and Val68Val rats differentially impacted *Bdnf* mRNA expression in grafted DA neurons. We found that approximately 87% of transplanted DA neurons expressed *Bdnf* mRNA in host subjects of both genotypes (Fig.

10b,c). Indeed, there was no difference in the percentage of grafted DA neurons expressing *Bdnf* mRNA between genotypes (mean percentage of DA neurons containing *Bdnf* mRNA \pm SEM: Val68Val: $87.55 \pm 3.408\%$; Met68Met: $87.27 \pm 1.751\%$; $t(10) = 0.07763$, $p = 0.9397$; Fig. 10c). There also was no difference in the level of *Bdnf* mRNA transcript in grafted DA neurons when transplanted into either Met68Met or Val68Val hosts ($t(9) = 0.2020$, $p = 0.8444$).

3.8.2. Met68Met host striatal neurons contain more *Trkb* mRNA than Val68Val striatal neurons in sham grafted subjects, but not in DA grafted subjects—

We next examined the impact of host genotype and the presence of grafted DA neurons on mRNA expression for the high affinity BDNF receptor, TrkB, in the host striatum. *Trkb* mRNA expression was quantified in the dorsolateral region of both the intact and lesioned striatum. In DA grafted subjects, *Trkb* mRNA expression was measured in the dorsolateral striatum adjacent to the grafts. As might be anticipated, in sham grafted subjects, striatal *Trkb* mRNA expression was significantly higher in Met68Met hosts than in their wild-type counterparts (Fig. 10d, e). This finding was consistent for intact and 6-OHDA lesioned striatum (two-way ANOVA $F(1,8) = 11.56$, $p = 0.0094$; Šídák's multiple comparisons test: Intact: $t(16) = 3.318$, $p = 0.0087$; Lesion: $t(16) = 2.553$, $p = 0.0421$). With the loss of nigral DA input to the striatum (a primary source of BDNF), there was an increase in *Trkb* mRNA expression with 6-OHDA lesion in Val68Val subjects (two-way ANOVA $F(1,8) = 10.42$, $p = 0.0121$; Šídák's multiple comparisons test: Val68Val: $t(8) = 2.818$, $p = 0.0446$; Met68Met: $t(8) = 1.746$, $p = 0.2238$). In the striatum of DA grafted rats there was no significant difference in *Trkb* mRNA expression between genotypes; curiously, this was also found to be true in the contralateral intact striatum (two-way ANOVA $F(1,9) = 0.2564$, $p = 0.6247$; Šídák's multiple comparisons test: Intact: $t(18) = 0.6221$, $p = 0.7899$; Lesion: $t(18) = 0.3204$, $p = 0.9387$); Fig. 10f,g).

4. Discussion

4.1. Renewed interest in clinical grafting trials: Are we ready?

Recent preclinical data from our laboratories (Collier et al., 2015) together with that from two milestone clinical reports (Li et al., 2016; Kordower et al., 2017) provide compelling and sobering evidence demonstrating that despite robust survival and extensive neurite outgrowth from grafted DA neurons, obstacle(s) remain that interfere with functional circuit restoration within the aged, parkinsonian brain. Currently, clinical grafting trials, refined by decades of research, are ongoing or planned for the near future (e.g., (Barker and Consortium, 2019), Clinical Trial Identifiers [NCT01898390](#), [NCT03309514](#), [NCT03119636](#), [NCT04146519](#)). However, as the primary clinical objective is to provide an additional treatment option for PD patients that is safe and effective, the question remains whether our current understanding of this experimental regenerative therapy is sufficient for safe and informed clinical practice. While the field of regenerative medicine has gained an understanding of the role of *global* risk factors in cell transplantation for PD, the current study is the first indicating the importance of understanding the role of individual *genetic* risk factors for this therapeutic approach.

4.2. The potential role of personalized medicine in clinical grafting trials

The potential importance of the findings reported here related to the rs6265 SNP and the clinical regenerative approach of cell transplantation in PD, whether it be through primary embryonic or stem cells, lies in the fact that it is estimated that approximately 20% of the worldwide human population possesses the Val66Met/rs6265 SNP in the *BDNF* gene, though there is much variability between populations (dbSNP, 2020). For example, while this SNP is uncommon in African populations (<5% Met allele frequency), it is extremely common in East Asian populations (up to 72% Met allele frequency) (dbSNP, 2020; Petryshen et al., 2010). Important to the current topic, BDNF promotes dendritic spine integrity as well as synapse development and maturation within the striatum (Lai and Ip, 2013; Zagrebelsky and Korte, 2014). It is also known to significantly impact graft-derived innervation following engraftment of embryonic VM neurons into parkinsonian rats (Yurek et al., 1996; Yurek et al., 1998) and differentiation and maturation of embryonic and adult neural stem/progenitor cells (Numakawa et al., 2017).

Given the relevant biology of this trophic factor and the prominence of rs6265 in the human population, we asked the question: Since there is a subpopulation of PD patients that does not respond well to DA neuron transplantation, and there is a subpopulation of PD patients that carries this SNP, could the Met risk allele make the striatum a less hospitable environment for transplanted DA neurons to make normal/meaningful connections? As detailed above, our data using the rs6265 knock-in rat model to test the hypothesis that dysfunctional BDNF associated with this SNP is an unrecognized contributor to suboptimal clinical benefit and development of graft-derived side-effects suggests that this common human SNP may undoubtedly impact functional outcome in clinical grafting trials in PD. In the following discussion, we highlight how the current data integrate with the current understanding of the biology of this SNP and provide novel insight on how this SNP might impact cell replacement strategies in PD.

4.3. Paradoxical enhancement of neurite outgrowth associated with the Met allele

Contrary to one aspect of our hypothesis, we found that parkinsonian Met68Met rats showed enhanced therapeutic efficacy evidenced by an earlier and more robust amelioration of LID behavior post-engraftment compared to wild-type Val68Val rats. In line with this, we discovered that rats homozygous for the Met allele displayed significantly enhanced neurite outgrowth derived from wild-type embryonic DA neurons compared to that seen in Val68Val hosts. While this discovery seemed paradoxical to what would be expected in an environment of diminished BDNF availability, the rs6265 risk allele has previously been indicated in enhanced recovery following stroke and traumatic brain injury (TBI) (Krueger et al., 2011; Qin et al., 2014; Failla et al., 2015). Interestingly, in a study using a rs6265 mouse model, Qin and colleagues (Qin et al., 2014) found, contrary to their hypothesis, that mice homozygous for the variant Met allele displayed better motor recovery after receiving a transient middle cerebral artery occlusion when compared to their wild-type counterparts. Further, Krueger and colleagues (Krueger et al., 2011) examined the recovery of executive functioning in Vietnam veterans who had sustained combat-related TBI. Though the authors initially hypothesized that the Val allele would promote recovery of executive functioning, it was the Met allele carriers who experienced better recovery of this behavioral measure. The

rs6265 SNP was also found to predict mortality in a longitudinal study in patients with severe TBI (Failla et al., 2015). In this study, Failla and colleagues examined patients receiving care for a closed-head injury, both acutely (0–7 days post-injury) and post-acutely (8–365 days post-injury). Unexpectedly, they found that Met allele carriers had greater survival probability at the acute timepoint compared to Val66Val subjects. Most recently, the Met allele has been found to be associated with enhanced neurite outgrowth of human induced pluripotent stem cell (iPSC)-derived spinal motor neurons (personal communication, Dr. Colin K. Franz, <https://www.abstractsonline.com/pp8/#!/7883/presentation/69599>) and excitatory cortical projection neurons (personal communication, Dr. Colin K. Franz, <https://www.abstractsonline.com/pp8/#!/7883/presentation/68155>) *in vitro*. In addition, neurite regeneration was enhanced following transection injury in human iPSC-derived motor neurons cultured in microfluidic chambers (personal communication, Dr. Colin K. Franz; <https://www.abstractsonline.com/pp8/#!/7883/presentation/69599>). In keeping with this observation in human iPSCs, enhanced peripheral axon regeneration has been observed in association with rs6265 both *in vivo* and in cultured dorsal root ganglion neurons in a mouse model of this SNP (McGregor and English, 2018).

Ultimately, considering the abundance of the rs6265 Met allele in the human population, it would seem illogical that such a common genetic variant is entirely disadvantageous (Di Pino et al., 2016). While an increasing collection of evidence suggests a beneficial role for the variant Met allele in axonal growth and regeneration, we show here that even wild-type neurons can be induced to develop this enhanced phenotype when transplanted ectopically into a Met allele-carrying host. In addition, despite the Met allele being associated with enhanced neurite outgrowth and enhanced functional benefit in our grafting study and in other conditions (Krueger et al., 2011; Qin et al., 2014; Failla et al., 2015), we provide the first evidence that an individual's genotype may also underlie development of aberrant mechanisms associated with GID behavioral phenotype.

4.4. The BDNF prodomain as a biologically active ligand: implications for maturation of neuronal circuitry

Historically, BDNF has been shown to have a direct impact on the morphological development of neurons, typically by promoting growth and branching of axon terminals and facilitating the establishment of mature neuronal circuitry (reviewed in (Cohen-Cory et al., 2010)). Why, then, a host environment with significantly reduced activity-dependent BDNF release would promote neurite outgrowth is a mystery. Indeed, the molecular mechanism underlying the paradoxical phenomena of increased neurite outgrowth and enhanced recovery from injury in association with the rs6265 Met allele is currently unknown. However, the extensive outgrowth that we observed from grafted DA neurons is reminiscent of the formation of extraneous neuronal processes and synapses during development that are later pruned back to facilitate the formation of functionally mature neuronal circuitry (Cowan et al., 1984; Low and Cheng, 2006). Recently, it has been shown that dendritically translated BDNF and its precursor, proBDNF, are crucially involved in synaptic maturation and pruning in developing hippocampal neurons (Orefice et al., 2016). Furthermore, BDNF and proBDNF have been extensively studied as modulators of synapse structure, maturation, and plasticity and are known to have opposing roles in this regard

(e.g., (Lai and Ip, 2013; Zagrebelsky and Korte, 2014; Park and Poo, 2013; Lu et al., 2005)). Specifically, whereas mature BDNF promotes dendritic spine formation and long-term potentiation (LTP), proBDNF promotes growth cone retraction, spine shrinkage, and long-term depression (LTD) (e.g., (Lu et al., 2005; Woo et al., 2005; Teng et al., 2005; Deinhardt et al., 2011; Koshimizu et al., 2009; Patterson et al., 1996; Korte et al., 1996; Rauskolb et al., 2010)). As BDNF signaling is tightly regulated, it is logical to assume that a disturbance in BDNF signaling may impact this intricate balance of synapse pruning and maturation in developing (grafted) neurons.

Recently, the BDNF prodomain, which is cleaved from proBDNF to produce the mature BDNF protein, has been implicated as another independent and biologically active ligand with modulatory effects at the synapse (Anastasia et al., 2013; Mizui et al., 2015; Guo et al., 2016; Giza et al., 2018). As reviewed in (Zanin et al., 2017), the first of these studies (Anastasia et al., 2013) revealed that the BDNF prodomain containing the variant Met allele induced growth cone retraction and collapse in cultured hippocampal neurons. The same group later showed that the Met-prodomain eliminated mature mushroom spines and reduced axonal projection density in ventral CA1 hippocampal (vCA1) neurons during peri-adolescence, whereas the wild-type Val-prodomain had no effect (Giza et al., 2018). Conversely, a separate group of researchers showed that the Val-prodomain facilitated LTD in the hippocampus, whereas the Met-prodomain completely prevented this effect (Mizui et al., 2015). Finally, in a report by a third group, the Val-prodomain reduced dendritic spine density in rat hippocampal neurons (Guo et al., 2016).

Much remains to be understood regarding the function of the BDNF prodomain as an independent ligand, especially in structures outside of the hippocampus, and how the rs6265 SNP impacts neuron and synapse function. However, these initial findings may still have important implications. Specifically, Giza and colleagues (Giza et al., 2018) concluded that the Met-prodomain, when applied to developing vCA1 neurons during peri-adolescence, rendered these neurons “underdeveloped,” thus preventing maturation of fear extinction circuitry in rs6265 Met allele carriers. Considering the compelling evidence that the prodomain may act as an independent and biologically active ligand with modulatory effects at the synapse, the current data could be hypothesized to suggest that the Met-prodomain prevents maturation and pruning of synaptic connectivity between grafted DA neurons and the host striatum.

4.5. Abnormal target plasticity: Evidence for aberrant graft-host synaptic connectivity in rs6265 SNP carriers

Structural changes mediated by DA depletion in the parkinsonian striatum have been postulated as potential contributors to GID development (reviewed in (Steece-Collier et al., 2012)). Specifically, it is known that striatal DA depletion causes morphological alterations to striatal MSNs (primary targets of grafted DA neurons) including dendritic spine loss, both in human PD patients and parkinsonian animal models (McNeill et al., 1988; Zaja-Milatovic et al., 2005; Stephens et al., 2005; Day et al., 2006; Neely et al., 2007; Villalba et al., 2009). Furthermore, preventing this loss of MSN spines with the calcium channel antagonist nimodipine reduces GID behavior in DA grafted rats (Soderstrom et al., 2010).

As described above, BDNF signaling is a potent modulator of spine and synapse dynamics in the striatum (Rauskolb et al., 2010; Saylor et al., 2006; Baquet et al., 2004; Li et al., 2012; Xie et al., 2010; Razgado-Hernandez et al., 2015) and corticostriatal plasticity (Jia et al., 2010). In a mouse model of the rs6265 *BDNF* SNP, Jing and colleagues (Jing et al., 2017) observed an increase in immature thin spines and a decrease in mature mushroom spines in the dorsolateral striatum of BDNF Met/Met mice, despite no change in total spine density. This phenomenon was also observed in cultured hippocampal neurons treated with the Met-prodomain (Giza et al., 2018). Moreover, in addition to its known role in impairment of cortical and hippocampal plasticity (Ninan et al., 2010; Bath et al., 2012; Pattwell et al., 2012; Galvin et al., 2015), the rs6265 SNP is also associated with impaired striatal plasticity (Jing et al., 2017). Based on the finding that total MSN spine density does not change with rs6265, the authors suggested that dendritic spine density *per se* may not contribute to the observed changes in striatal plasticity (Jing et al., 2017). However, the shift in spine phenotype from mature to immature suggests that the development of functionally mature synapses may be impaired in rs6265 striatum.

In the current study, we quantified presumed synaptic connections between MSN dendritic spines (i.e., synaptopodin/SP) and grafted DA neurons. Interestingly, despite similar numbers of these graft-host synaptic appositions, only wild-type rats exhibited a significant decrease in LID behavior with increased density of synaptic contacts, as expected per (Collier et al., 2015). This evidence suggests that grafted DA neurons in Met68Met rats may not be capable of establishing functionally appropriate/mature synaptic contacts with striatal dendritic spines, despite contact densities similar in number to that of wild-type rats. We propose that this may be due to structural differences in the MSN spines available for establishing connections and/or an inability to develop functionally mature connections with grafted cells, and that the enhanced amelioration of LID observed in Met68Met rats may occur through a separate underlying mechanism (e.g., autocrine release of DA from the extensive neurite network).

4.6. VGLUT2 expression indicative of immature phenotype in transplanted DA neurons: A molecular driver of GID?

In the normal adult striatum, nigrostriatal DA synapses exhibit ultrastructural features common to symmetric (Gray type-II) synapses (Freund et al., 1984; Moss and Bolam, 2008; Pickel et al., 1981). Interestingly, atypical asymmetric (Gray type-I/excitatory) synapses formed by TH⁺ fibers have been documented postmortem in DA grafts from PD patients (Kordower et al., 1996), parkinsonian non-human primates (Leranth et al., 1998), and parkinsonian rats (Soderstrom et al., 2008). In parkinsonian rats, we previously reported that asymmetric synapses made by grafted DA neurons are associated with GID (Soderstrom et al., 2008). In the current study, grafted Met68Met rats were the only group to develop significant GID, despite the presence of a widespread graft which does not typically cause GID in wild-type rats (Maries et al., 2006). Accordingly, we reasoned that if GID in Met68Met hosts are associated with asymmetric (presumed excitatory) DA synapses, these DA neurons should show neurochemical evidence of DA-glutamate co-transmission. As such, the grafted DA neurons should contain *Vglut2* mRNA and VGLUT2 protein.

During normal development, nigral DA neurons do indeed express *Vglut2* mRNA and VGLUT2 protein and show evidence of DA-glutamate co-transmission, a phenotype that typically disappears with maturation (for review (El Mestikawy et al., 2011)). We show here the first neurochemical evidence supporting the fact that grafted DA neurons maintain this immature phenotype well into a timeframe that should be associated with maturation and loss of DA-glutamate co-expression (Prakash and Wurst, 2006). Indeed, in our study, approximately 60% of transplanted DA neurons contained *Vglut2* mRNA, and this occurred regardless of host genotype, suggesting this is inherent to the graft. This contrasts the <5% found in mature SN and ~25% in mature VTA DA neurons that we (Fig 6) and others (e.g., (Morales and Margolis, 2017; Morales and Root, 2014)) have found.

As would be expected in DA neurons expressing *Vglut2* mRNA, we provide evidence of VGLUT2 protein found within transplanted DA fibers. Similar to *Vglut2* mRNA in mature SN and VTA, there was significantly less VGLUT2 in mature nigral DA fibers projecting to the striatum in naïve adult rats. While we did not perform ultrastructural analyses in the current study, we provide neurochemical evidence that grafted DA neurons create presumed excitatory (glutamatergic) synapses in the grafted striatum as evidenced by VGLUT2 *within* DA neurites making close ($< 0.6 \mu\text{m}$) appositions with PSD95 in the host striatum. While we appreciate that synapses are orders of magnitude smaller, we used a semi-automated approach that combines triple label immunofluorescence and high-resolution confocal microscopy to provide the first evidence of neurochemical signatures of excitatory synapses made by DA neurons in the grafted parkinsonian striatum. In keeping with our previously reported data showing a positive trend between ultrastructurally identified asymmetric DA synapses and levodopa-mediated GID (Soderstrom et al., 2008), in the present study, we show that amphetamine-mediated GID is significantly, positively associated with asymmetric DA synapses, but interestingly *only in Met68Met rats*.

Again, as wild-type rats do not typically develop GID with wide-spread DA grafts (Maries et al., 2006), the lack of correlation between asymmetric DA synapses and GID in grafted Val68Val subjects was not unexpected. However, it is notable that the lack of association between these two factors occurred in Val68Val rats despite similar levels of VGLUT2 expression between genotypes. We propose here that this collective evidence is suggestive of synaptic rewiring or “miswiring” between transplanted DA neurons and the host brain in Met68Met subjects – perhaps reflective of an inability to establish and/or maintain mature synaptic connectivity - which in turn promotes aberrant graft-induced side-effects.

4.7. Corticostriatal connections with grafted cells

Previous evidence from our group (Soderstrom et al., 2008) revealed a significant positive correlation between total levodopa-mediated GID severity and the proportion of aberrant asymmetric synapses onto grafted DA neurons in parkinsonian rats. These connections were presumed to be new corticostriatal inputs onto the grafted DA neurons, which were themselves making atypical excitatory (dopaminergic/glutamatergic) contacts onto host striatum neurons, and were hypothesized to create a nidus of aberrant excitatory drive leading to GID (Soderstrom et al., 2008). Accordingly, in the current study, we examined

whether GID behavior in Met68Met rats correlated with excitatory VGLUT1-labeled corticostriatal input onto grafted DA neurons.

In contrast to our earlier findings, we did not find a correlation between GID and corticostriatal connections in grafted rats of either genotype. This may be due to the fact that in the present study we analyzed VGLUT1 input onto grafted DA fibers extending into the striatal parenchyma, while our previous electron microscopic evidence found that these connections occurred more frequently on grafted DA somas and proximal dendrites (Soderstrom et al., 2008). While the precise relationship of VGLUT1 to GID behaviors remains unclear, the current study did reveal that there was a significant increase in corticostriatal VGLUT1 input onto DA fibers in the grafted vs intact striatum in Met68Met rats that express this behavioral phenotype, but not in Val68Val rats. While the implications associated with this phenomenon of elevated corticostriatal input onto DA fibers in Met68Met GID-expressing rats are uncertain, it is known from the rs6265 mouse model that there is a basal elevation of glutamatergic neurotransmission in dorsolateral striatum of subjects with the Met risk allele (Jing et al., 2017). A similar enhancement of glutamatergic neurotransmission in the striatum has been observed in animal models for Huntington's disease where BDNF availability is decreased (Milnerwood and Raymond, 2010). The increased strength of glutamatergic synapses in the striatum has been suggested to play a role in aberrant plasticity involved with the enhancement of basal ganglia related behaviors such as anxiety and drug-seeking behaviors in Met allele carriers (for review (Jing et al., 2017)). Given the proposed similarities in aberrant striatal plasticity mechanisms between addiction and dyskinesias (e.g., (Steece-Collier et al., 2020)), it is reasonable to hypothesize that excessive corticostriatal neurotransmission could be a mechanism contributing to the expression of GID behaviors in subjects with the Met allele.

4.8. Cell composition in VM grafts: Serotonin neurons and implications for dyskinetic behavior

4.8.1. Serotonin neurons and LID—In the parkinsonian striatum, levodopa is converted to DA by the enzyme aromatic amino acid decarboxylase (AADC) within remaining striatal DA terminals. However, as striatal DA terminals are depleted in advancing PD, this function is maintained instead by 5-HT neurons of the dorsal raphe nucleus (DRN) that sprout into the parkinsonian striatum. Specifically, it is known that serotonergic innervation of the striatum is markedly increased following DA depletion (Maeda et al., 2003; Maeda et al., 2005) and levodopa treatment (Rylander et al., 2010) and that DRN 5-HT neurons contain AADC and the vesicular monoamine transporter 2 (VMAT2). Therefore, endogenous striatal 5-HT terminals are capable of taking up exogenous levodopa and subsequently synthesizing, storing, and releasing DA as a “false neurotransmitter” after levodopa administration (reviewed in detail elsewhere, e. g., (Steece-Collier et al., 2012; Shin et al., 2012b; Munoz et al., 2020)). Unlike DA neurons, however, 5-HT neurons do not possess mechanisms of regulatory feedback (i.e., DA D2 autoreceptors and the DA transporter). Thus, the release of DA from 5-HT terminals following levodopa administration is unregulated and non-physiological, which is thought to contribute to dyskinesogenesis (e.g., (Carta et al., 2007)). Indeed, in support of this theory, it has been

shown that viral vector-mediated expression of the DA D2 autoreceptor in DRN 5-HT neurons blocks LID in parkinsonian rats (Sellnow et al., 2019).

4.8.2. Serotonin neurons and GID—In addition to their role in contributing to LID, 5-HT neurons have been implicated, with some controversy, as a causative factor in the development of GID in grafted subjects (Politis et al., 2010; Politis et al., 2011). This contention is supported by evidence indicating that GID were markedly reduced in three grafted PD patients with extensive graft-derived serotonergic hyperinnervation when treated with buspirone, a 5-HT_{1A} partial agonist that also displays DA D2 receptor (D2R) antagonistic properties (Steece-Collier et al., 2012; Politis et al., 2010; Politis et al., 2011). However, the role of 5-HT neurons – both graft-derived and endogenous – in GID development has yet to be conclusively defined. For instance, the presence (often in abundance) of 5-HT neurons in transplants has been observed in the absence of GID in VM grafted PD patients (Mendez et al., 2008; Cooper et al., 2009). Furthermore, additional evidence strongly suggests that buspirone suppresses GID through its action as a DA D2R antagonist, rather than its interaction with the 5-HT_{1A} receptor (Shin et al., 2012a; Shin et al., 2014). Indeed, buspirone was initially developed as an antipsychotic drug based on its interaction with the DA D2R (New, 1990) and is known to exhibit varying levels of antagonistic affinity for DA receptors D1-D4 (Dhavalshankh et al., 2007; Loane and Politis, 2012; Bergman et al., 2013). Ultimately, though the topic remains a matter of debate, the majority of available evidence is supportive of a major role for the DA system in the development of GID, with a modulatory role for the 5-HT system (Lane et al., 2009a; Garcia et al., 2012; Aldrin-Kirk et al., 2016; Tronci et al., 2015).

In keeping with the current dogma regarding 5-HT neurons and LID causation (e.g., (Rylander et al., 2010; Carta et al., 2007; Sellnow et al., 2019)), we observed a positive trend between the 5-HT/DA cell ratio and LID in wild-type rats. However, data from our current study do *not* support a role of graft-derived 5-HT neurons in the expression of GID behaviors since there was a similar proportion of 5-HT/DA neurons in both Met68Met and Val68Val rats, as well as a lack of correlation of this behavior with 5-HT/DA ratios in both genotypes. Despite this finding, it may be of interest in future studies to consider whether there are differences in 5-HT and VGLUT3 colocalization between genotypes and whether this parameter correlates with GID and/or LID. Similar to DA neurons colocalizing VGLUT2, 5-HT neurons, even in the mature brain, co-express vesicular glutamate transporter 3 (VGLUT3) which has been proposed to be involved in the phenomenon called “vesicular synergy” that results in increased extracellular 5-HT (El Mestikawy et al., 2011). Thus, understanding whether such a mechanism correlates with GID and/or LID may be warranted (Steece-Collier et al., 2012).

4.9. Conclusion & future directions

In this era of personalized medicine, understanding both global (e.g., aging) and specific (e.g., rs6265 SNP) factors that might impact efficacy of clinical interventions such as cell replacement therapy could provide significant advances in the field of regenerative medicine. The current studies, performed in mature adult (6 mos at time of grafting) rats homozygous for the rs6265 SNP, were undertaken as proof-of-principle studies to determine whether the

genotype that would produce the largest reduction in BDNF release would have any impact on graft function or dysfunction compared to wild-type rats. These experiments provide clear evidence that the Met68Met genotype in the host significantly impacts DA graft efficacy in this model. While suggesting some novel mechanisms associated with DA graft function and/or dysfunction in association with the rs6265 SNP as discussed above, the current studies leave many questions unanswered. Nevertheless, these novel studies provide an important foundation for an abundance of future investigations. For example, as the present study clearly demonstrates the significant impact of *host* genotype on wild-type donor cells, additional studies will be essential to examine the role of *graft* genotype. In addition, while the inclusion of heterozygous Val/Met subjects was beyond the scope of the present investigation, this is highly warranted for future studies. Finally, based on the known association of advanced age with PD and poor graft efficacy (Freed et al., 2001), we have an ongoing study in our rs6265 rats in which we are examining the interaction of advancing age with this SNP. We posit that a combination of future data provided from our ongoing studies in aged (15 mos at time of grafting) parkinsonian Met68Met and wild-type rats together with that which might be obtained from grafted PD patients will be needed to provide the most comprehensive understanding of how these two factors, one global and one genetic, impact therapeutic outcome for this experimental therapy.

Indeed, to the best of our knowledge, PD patients and transplanted donor cells are not currently genotyped for this SNP. Notably, a large clinical grafting study is currently in the recruiting phase in China (Clinical Trial Identifier: [NCT03119636](https://clinicaltrials.gov/ct2/show/study/NCT03119636)). Considering that the rs6265 SNP is highly prevalent in East Asian countries, with some allelic frequency estimates as high as 72% (Petryshen et al., 2010), the findings of the current study suggest that it would be prudent to genotype the clinical participants so the impact of the rs6265 SNP may be considered during interpretation of the study results. While the current studies are most relevant to PD, data from these studies together with those from human TBI subjects with the Met genotype and the rs6265 mouse stroke model (Krueger et al., 2011; Qin et al., 2014; Failla et al., 2015) suggest that understanding how to harness the “good” phenotype (i.e., enhanced neurite outgrowth and functional benefit) while subverting the “bad” phenotype (i.e., motor dysfunction/GID; anxiety and depression (Jing et al., 2017)) associated with the Met allele could provide a means for optimizing not only the clinical regenerative medicine approach of cell transplantation for PD but also treatment for a variety of traumatic, degenerative, and/or developmental maladies.

Supplementary Material

Refer to Web version on PubMed Central for supplementary material.

Acknowledgments

This study was supported by the National Institute of Neurological Disorders and Stroke grant NS105826 (KSC, CES, TJC) and the Michigan Parkinson Foundation (KSC, NMM). The authors have no other conflicts of interest to report. We would like to acknowledge the excellent technical assistance of Brian Daley, BS, Christopher Kemp, MS, and Amandine Roux, PhD. We also thank Colin K. Franz, MD, PhD, Shirley Ryan AbilityLab, Department of Physical Medicine and Rehabilitation, and Neurology, Northwestern University Feinberg School of Medicine, Chicago, IL for his unpublished research communication, and Margaret Fahnestock, PhD, McMaster University Health Sciences Center, Hamilton, Ontario, Canada for her expertise and guidance with BDNF biology.

References

- Adachi N, Numakawa T, Richards M, Nakajima S, Kunugi H, 2014 New insight in expression, transport, and secretion of brain-derived neurotrophic factor: Implications in brain-related diseases. *World J. Biol. Chem* 5, 409–428. <https://10.4331/wjbc.v5.i4.409>.
- Aid T, Kazantseva A, Piirsoo M, Palm K, Timmusk T, 2007 Mouse and rat bdnf gene structure and expression revisited. *J. Neurosci. Res* 85, 525–535. <https://10.1002/jnr.21139>. [PubMed: 17149751]
- Aldrin-Kirk P, Heuer A, et al., 2016 DREADD modulation of transplanted DA neurons reveals a novel parkinsonian dyskinesia mechanism mediated by the serotonin 5-HT6 receptor. *Neuron* 90, 955–968. <https://10.1016/j.neuron.2016.04.017>. [PubMed: 27161524]
- Altar CA, DiStefano PS, 1998 Neurotrophin trafficking by anterograde transport. *Trends Neurosci.* 21, 433–437. [https://10.1016/s0166-2236\(98\)01273-9](https://10.1016/s0166-2236(98)01273-9). [PubMed: 9786341]
- Altar CA, Cai N, et al., 1997 Anterograde transport of brain-derived neurotrophic factor and its role in the brain. *Nature* 389, 856–860. <https://10.1038/39885>. [PubMed: 9349818]
- Anastasia A, Deinhardt K, et al., 2013 Val66met polymorphism of bdnf alters prodomain structure to induce neuronal growth cone retraction. *Nat. Commun* 4, 2490 <https://10.1038/ncomms3490>. [PubMed: 24048383]
- Baj G, Carlino D, Gardossi L, Tongiorgi E, 2013 Toward a unified biological hypothesis for the bdnf val66met-associated memory deficits in humans: A model of impaired dendritic mRNA trafficking. *Front. Neurosci* 7, 188 <https://10.3389/fnins.2013.00188>. [PubMed: 24198753]
- Baquet ZC, Gorski JA, Jones KR, 2004 Early striatal dendrite deficits followed by neuron loss with advanced age in the absence of anterograde cortical brain-derived neurotrophic factor. *J. Neurosci* 24, 4250–4258. <https://10.1523/JNEUROSCI.3920-03.2004>. [PubMed: 15115821]
- Barker RA, Consortium T, 2019 Designing stem-cell-based dopamine cell replacement trials for parkinson's disease. *Nat. Med* 25, 1045–1053. <https://10.1038/s41591-019-0507-2>. [PubMed: 31263283]
- Bastide MF, Meissner WG, et al., 2015 Pathophysiology of l-dopa-induced motor and non-motor complications in parkinson's disease. *Prog. Neurobiol* 132, 96–168. <https://10.1016/j.pneurobio.2015.07.002>. [PubMed: 26209473]
- Bath KG, Jing DQ, et al., 2012 Bdnf val66met impairs fluoxetine-induced enhancement of adult hippocampus plasticity. *Neuropsychopharmacology* 37, 1297–1304. <https://10.1038/npp.2011.318>. [PubMed: 22218094]
- Baydyuk M, Xu B, 2014 Bdnf signaling and survival of striatal neurons. *Front. Cell. Neurosci* 8, 254 <https://10.3389/fncel.2014.00254>. [PubMed: 25221473]
- Belmer A, Klenowski PM, Patkar OL, Bartlett SE, 2017 Mapping the connectivity of serotonin transporter immunoreactive axons to excitatory and inhibitory neurochemical synapses in the mouse limbic brain. *Brain Struct. Funct* 222, 1297–1314. <https://10.1007/s00429-016-1278-x>. [PubMed: 27485750]
- Bergman J, Roof RA, et al., 2013 Modification of cocaine self-administration by buspirone (buspar(r)): Potential involvement of d3 and d4 dopamine receptors. *Int. J. Neuropsychopharmacol* 16, 445–458. <https://10.1017/S1461145712000661>. [PubMed: 22827916]
- Carta M, Carlsson T, Kirik D, Bjorklund A, 2007 Dopamine released from 5-HT terminals is the cause of l-dopa-induced dyskinesia in parkinsonian rats. *Brain* 130, 1819–1833. <https://10.1093/brain/awm082>. [PubMed: 17452372]
- Cenci MA, Crossman AR, 2018 Animal models of l-dopa-induced dyskinesia in parkinson's disease. *Mov. Disord* 33, 889–899. <https://10.1002/mds.27337>. [PubMed: 29488257]
- Chen X, Nelson CD, et al., 2011 PSD-95 is required to sustain the molecular organization of the postsynaptic density. *J. Neurosci* 31, 6329–6338. <https://10.1523/JNEUROSCI.5968-10.2011>. [PubMed: 21525273]
- Chen ZY, Jing D, et al., 2006 Genetic variant bdnf (val66met) polymorphism alters anxiety-related behavior. *Science* 314, 140–143. <https://10.1126/science.1129663>. [PubMed: 17023662]
- Cohen-Cory S, Kidane AH, Shirkey NJ, Marshak S, 2010 Brain-derived neurotrophic factor and the development of structural neuronal connectivity. *Dev Neurobiol* 70, 271–288. <https://10.1002/dneu.20774>. [PubMed: 20186709]

- Collier TJ, Sortwell CE, Daley BF, 1999 Diminished viability, growth, and behavioral efficacy of fetal dopamine neuron grafts in aging rats with long-term dopamine depletion: An argument for neurotrophic supplementation. *J. Neurosci* 19, 5563–5573. [PubMed: 10377363]
- Collier TJ, O'Malley J, et al., 2015 Interrogating the aged striatum: Robust survival of grafted dopamine neurons in aging rats produces inferior behavioral recovery and evidence of impaired integration. *Neurobiol. Dis* 77, 191–203. <https://10.1016/j.nbd.2015.03.005>. [PubMed: 25771169]
- Collier TJ, Sortwell CE, Mercado NM, Steece-Collier K, 2019 Cell therapy for parkinson's disease: Why it doesn't work every time. *Mov. Disord* 34, 1120–1127. <https://10.1002/mds.27742>. [PubMed: 31234239]
- Cooper O, Astradsson A, et al., 2009 Lack of functional relevance of isolated cell damage in transplants of parkinson's disease patients. *J. Neurol* 256 (Suppl. 3), 310–316. <https://10.1007/s00415-009-5242-z>. [PubMed: 19711122]
- Cowan WM, Fawcett JW, O'Leary DD, Stanfield BB, 1984 Regressive events in neurogenesis. *Science* 225, 1258–1265. <https://10.1126/science.6474175>. [PubMed: 6474175]
- Day M, Wang Z, et al., 2006 Selective elimination of glutamatergic synapses on striatopallidal neurons in parkinson disease models. *Nat. Neurosci* 9, 251–259. <https://10.1038/nn1632>. [PubMed: 16415865]
- dbSNP, 2020 Reference snp (rs) report: Rs6265. Available from. http://www.ncbi.nlm.nih.gov/SNP/snp_ref.cgi?searchType=ad hoc_search&type=rs&rs=rs6265
- Deinhardt K, Kim T, et al., 2011 Neuronal growth cone retraction relies on proneurotrophin receptor signaling through rac. *Sci. Signal* 4 ra82 <https://10.1126/scisignal.2002060>. [PubMed: 22155786]
- Dhavalshankh AG, Jadhav SA, et al., 2007 Effects of buspirone on dopamine dependent behaviours in rats. *Indian J. Physiol. Pharmacol* 51, 375–386. [PubMed: 18476392]
- Di Pino G, Pellegrino G, et al., 2016 Val66met bdnf polymorphism implies a different way to recover from stroke rather than a worse overall recoverability. *Neurorehabil. Neural Repair* 30, 3–8. <https://10.1177/1545968315583721>. [PubMed: 25896987]
- Dunnett SB, Bjorklund A, Stenevi U, Iversen SD, 1981 Behavioural recovery following transplantation of substantia nigra in rats subjected to 6-ohda lesions of the nigrostriatal pathway. I. Unilateral lesions. *Brain Res.* 215, 147–161. [https://10.1016/0006-8993\(81\)90498-4](https://10.1016/0006-8993(81)90498-4). [PubMed: 7260584]
- Egan MF, Kojima M, et al., 2003 The bdnf val66met polymorphism affects activity-dependent secretion of bdnf and human memory and hippocampal function. *Cell* 112, 257–269. [https://10.1016/s0092-8674\(03\)00035-7](https://10.1016/s0092-8674(03)00035-7). [PubMed: 12553913]
- El Mestikawy S, Wallen-Mackenzie A, Fortin GM, Descarries L, Trudeau LE, 2011 From glutamate co-release to vesicular synergy: vesicular glutamate transporters. *Nat. Rev. Neurosci* 12, 204–216. <https://10.1038/nrn2969>. [PubMed: 21415847]
- Failla MD, Kumar RG, et al., 2015 Variation in the bdnf gene interacts with age to predict mortality in a prospective, longitudinal cohort with severe tbi. *Neurorehabil. Neural Repair* 29, 234–246. <https://10.1177/1545968314542617>. [PubMed: 25063686]
- Fischer DL, Auinger P, et al., 2018 Bdnf variant is associated with milder motor symptom severity in early-stage parkinson's disease. *Parkinsonism Relat. Disord* 53, 70–75. <https://10.1016/j.parkreldis.2018.05.003>. [PubMed: 29759928]
- Fischer DL, Auinger P, et al., 2020 Bdnf rs6265 variant alters outcomes with levodopa in early-stage parkinson's disease. *Neurotherapeutics* (in press).
- Foltynie T, Cheeran B, et al., 2009 Bdnf val66met influences time to onset of levodopa induced dyskinesia in parkinson's disease. *J. Neurol. Neurosurg. Psychiatry* 80, 141–144. <https://10.1136/jnnp.2008.154294>. [PubMed: 18977816]
- Freed CR, Greene PE, et al., 2001 Transplantation of embryonic dopamine neurons for severe parkinson's disease. *N. Engl. J. Med* 344, 710–719. <https://10.1056/NEJM200103083441002>. [PubMed: 11236774]
- Freund TF, Powell JF, Smith AD, 1984 Tyrosine hydroxylase-immunoreactive boutons in synaptic contact with identified striatonigral neurons, with particular reference to dendritic spines. *Neuroscience* 13, 1189–1215. [https://10.1016/0306-4522\(84\)90294-x](https://10.1016/0306-4522(84)90294-x). [PubMed: 6152036]

- Galvin C, Lee FS, Ninan I, 2015 Alteration of the centromedial amygdala glutamatergic synapses by the bdnf val66met polymorphism. *Neuropsychopharmacology* 40, 2269–2277. <https://10.1038/npp.2015.76>. [PubMed: 25786582]
- Garcia J, Carlsson T, Dobrossy M, Nikkhah G, Winkler C, 2012 Impact of dopamine versus serotonin cell transplantation for the development of graft-induced dyskinesia in a rat parkinson model. *Brain Res.* 1470, 119–129. <https://10.1016/j.brainres.2012.06.029>. [PubMed: 22759908]
- Giza JI, Kim J, et al., 2018 The bdnf val66met prodomain disassembles dendritic spines altering fear extinction circuitry and behavior. *Neuron* 99 (163–178), e6 <https://10.1016/j.neuron.2018.05.024>.
- Gombash SE, Manfredsson FP, et al., 2014 Neuroprotective potential of pleiotrophin overexpression in the striatonigral pathway compared with overexpression in both the striatonigral and nigrostriatal pathways. *Gene Ther.* 21, 682–693. <https://10.1038/gt.2014.42>. [PubMed: 24807806]
- Guo J, Ji Y, et al., 2016 Bdnf pro-peptide regulates dendritic spines via caspase-3. *Cell Death Dis.* 7, e2264 <https://10.1038/cddis.2016.166>. [PubMed: 27310873]
- Hagell P, Cenci MA, 2005 Dyskinesias and dopamine cell replacement in parkinson's disease: a clinical perspective. *Brain Res. Bull* 68, 4–15. <https://10.1016/j.brainresbull.2004.10.013>. [PubMed: 16324999]
- Hagell P, Piccini P, et al., 2002 Dyskinesias following neural transplantation in parkinson's disease. *Nat. Neurosci* 5, 627–628. <https://10.1038/nm863>. [PubMed: 12042822]
- Hauser RA, Auinger P, Oakes D, 2009 Levodopa response in early parkinson's disease. *Mov. Disord* 24, 2328–2336. <https://10.1002/mds.22759>. [PubMed: 19908302]
- Hoglinger GU, Widmer HR, et al., 2001 Influence of time in culture and bdnf pretreatment on survival and function of grafted embryonic rat ventral mesencephalon in the 6-ohda rat model of parkinson's disease. *Exp. Neurol* 167, 148–157. <https://10.1006/exnr.2000.7546>. [PubMed: 11161602]
- Iascone DM, Li Y, et al., 2020 Whole-neuron synaptic mapping reveals spatially precise excitatory/inhibitory balance limiting dendritic and somatic spiking. *Neuron* 106 (566–578), e8 <https://10.1016/j.neuron.2020.02.015>.
- Jia Y, Gall CM, Lynch G, 2010 Presynaptic bdnf promotes postsynaptic long-term potentiation in the dorsal striatum. *J. Neurosci* 30, 14440–14445. <https://10.1523/JNEUROSCI.3310-10.2010>. [PubMed: 20980601]
- Jing D, Lee FS, Ninan I, 2017 The bdnf val66met polymorphism enhances glutamatergic transmission but diminishes activity-dependent synaptic plasticity in the dorsolateral striatum. *Neuropharmacology* 112, 84–93. <https://10.1016/j.neuropharm.2016.06.030>. [PubMed: 27378336]
- Konradi C, Westin JE, et al., 2004 Transcriptome analysis in a rat model of l-dopa-induced dyskinesia. *Neurobiol. Dis* 17, 219–236. <https://10.1016/j.nbd.2004.07.005>. [PubMed: 15474360]
- Kordower JH, Rosenstein JM, et al., 1996 Functional fetal nigral grafts in a patient with parkinson's disease: Chemoanatomic, ultrastructural, and metabolic studies. *J. Comp. Neurol* 370, 203–230. [https://10.1002/\(SICI\)1096-9861\(19960624\)370:2<203::AID-CNE6>3.0.CO;2-6](https://10.1002/(SICI)1096-9861(19960624)370:2<203::AID-CNE6>3.0.CO;2-6). [PubMed: 8808731]
- Kordower JH, Goetz CG, et al., 2017 Robust graft survival and normalized dopaminergic innervation do not obligate recovery in a parkinson disease patient. *Ann. Neurol* 81 (1), 46–57. <https://10.1002/ana.24820>. [PubMed: 27900791]
- Korte M, Griesbeck O, et al., 1996 Virus-mediated gene transfer into hippocampal ca1 region restores long-term potentiation in brain-derived neurotrophic factor mutant mice. *Proc. Natl. Acad. Sci. U. S. A* 93, 12547–12552. <https://10.1073/pnas.93.22.12547>. [PubMed: 8901619]
- Koshimizu H, Kiyosue K, et al., 2009 Multiple functions of precursor bdnf to cns neurons: negative regulation of neurite growth, spine formation and cell survival. *Mol Brain* 2, 27 <https://10.1186/1756-6606-2-27>. [PubMed: 19674479]
- Krueger F, Pardini M, et al., 2011 The role of the met66 brain-derived neurotrophic factor allele in the recovery of executive functioning after combat-related traumatic brain injury. *J. Neurosci* 31, 598–606. <https://10.1523/JNEUROSCI.1399-10.2011>. [PubMed: 21228168]
- Lai KO, Ip NY, 2013 Structural plasticity of dendritic spines: The underlying mechanisms and its dysregulation in brain disorders. *Biochim. Biophys. Acta* 1832, 2257–2263. <https://10.1016/j.bbadis.2013.08.012>. [PubMed: 24012719]

- Lane EL, Winkler C, Brundin P, Cenci MA, 2006 The impact of graft size on the development of dyskinesia following intrastriatal grafting of embryonic dopamine neurons in the rat. *Neurobiol. Dis* 22, 334–345. <https://10.1016/j.nbd.2005.11.011>. [PubMed: 16406222]
- Lane EL, Brundin P, Cenci MA, 2009a Amphetamine-induced abnormal movements occur independently of both transplant- and host-derived serotonin innervation following neural grafting in a rat model of parkinson's disease. *Neurobiol. Dis* 35, 42–51. <https://10.1016/j.nbd.2009.03.014>. [PubMed: 19361557]
- Lane EL, Vercammen L, Cenci MA, Brundin P, 2009b Priming for l-dopa-induced abnormal involuntary movements increases the severity of amphetamine-induced dyskinesia in grafted rats. *Exp. Neurol* 219, 355–358. <https://10.1016/j.expneurol.2009.04.010>. [PubMed: 19393238]
- Lee CS, Cenci MA, Schulzer M, Bjorklund A, 2000 Embryonic ventral mesencephalic grafts improve levodopa-induced dyskinesia in a rat model of parkinson's disease. *Brain* 123 (Pt 7), 1365–1379. [PubMed: 10869049]
- Leranth C, Sladek JR Jr., Roth RH, Redmond DE Jr., 1998 Efferent synaptic connections of dopaminergic neurons grafted into the caudate nucleus of experimentally induced parkinsonian monkeys are different from those of control animals. *Exp. Brain Res* 123, 323–333. [PubMed: 9860271]
- Li M, Dai FR, et al., 2012 Infusion of bdnf into the nucleus accumbens of aged rats improves cognition and structural synaptic plasticity through pi3k-ilk-akt signaling. *Behav. Brain Res* 231, 146–153. <https://10.1016/j.bbr.2012.03.010>. [PubMed: 22446058]
- Li W, Englund E, et al., 2016 Extensive graft-derived dopaminergic innervation is maintained 24 years after transplantation in the degenerating parkinsonian brain. *Proc. Natl. Acad. Sci. U. S. A* 113, 6544–6549. <https://10.1073/pnas.1605245113>. [PubMed: 27140603]
- Lindvall O, 2015 Treatment of parkinson's disease using cell transplantation. *Philos. Trans. R. Soc. Lond. Ser. B Biol. Sci* 370, 20140370 <https://10.1098/rstb.2014.0370>. [PubMed: 26416681]
- Loane C, Politis M, 2012 Buspirone: what is it all about? *Brain Res.* 1461, 111–118. <https://10.1016/j.brainres.2012.04.032>. [PubMed: 22608068]
- Low LK, Cheng HJ, 2006 Axon pruning: an essential step underlying the developmental plasticity of neuronal connections. *Philos. Trans. R. Soc. Lond. Ser. B Biol. Sci* 361, 1531–1544. <https://10.1098/rstb.2006.1883>. [PubMed: 16939973]
- Lu B, Pang PT, Woo NH, 2005 The yin and yang of neurotrophin action. *Nat. Rev. Neurosci* 6, 603–614. <https://10.1038/nrn1726>. [PubMed: 16062169]
- Maeda T, Kannari K, et al., 2003 Rapid induction of serotonergic hyperinnervation in the adult rat striatum with extensive dopaminergic denervation. *Neurosci. Lett* 343, 17–20. [https://10.1016/s0304-3940\(03\)00295-7](https://10.1016/s0304-3940(03)00295-7). [PubMed: 12749987]
- Maeda T, Nagata K, Yoshida Y, Kannari K, 2005 Serotonergic hyperinnervation into the dopaminergic denervated striatum compensates for dopamine conversion from exogenously administered l-dopa. *Brain Res.* 1046, 230–233. <https://10.1016/j.brainres.2005.04.019>. [PubMed: 15894297]
- Mallei A, Baj G, et al., 2015 Expression and dendritic trafficking of bdnf-6 splice variant are impaired in knock-in mice carrying human bdnf val66met polymorphism. *Int. J. Neuropsychopharmacol* 18 <https://10.1093/ijnp/pyv069>.
- Mariani S, Ventriglia M, et al., 2015 Meta-analysis study on the role of bone-derived neurotrophic factor val66met polymorphism in parkinson's disease. *Rejuvenation Res.* 18, 40–47. <https://10.1089/rej.2014.1612>. [PubMed: 25431370]
- Maries E, Kordower JH, et al., 2006 Focal not widespread grafts induce novel dyskinetic behavior in parkinsonian rats. *Neurobiol. Dis* 21, 165–180. <https://10.1016/j.nbd.2005.07.002>. [PubMed: 16095907]
- McGregor CE, English AW, 2018 The role of bdnf in peripheral nerve regeneration: activity-dependent treatments and val66met. *Front. Cell. Neurosci* 12, 522 <https://10.3389/fncel.2018.00522>. [PubMed: 30687012]
- McNeill TH, Brown SA, Rafols JA, Shoulson I, 1988 Atrophy of medium spiny i striatal dendrites in advanced parkinson's disease. *Brain Res.* 455, 148–152. [PubMed: 3416180]

- Mendez I, Vinuela A, et al., 2008 Dopamine neurons implanted into people with parkinson's disease survive without pathology for 14 years. *Nat. Med* 14, 507–509. <https://10.1038/nm1752>. [PubMed: 18391961]
- Milnerwood AJ, Raymond LA, 2010 Early synaptic pathophysiology in neurodegeneration: insights from huntington's disease. *Trends Neurosci.* 33, 513–523. <https://10.1016/j.tins.2010.08.002>. [PubMed: 20850189]
- Mizui T, Ishikawa Y, et al., 2015 Bdnf pro-peptide actions facilitate hippocampal ltp and are altered by the common bdnf polymorphism val66met. *Proc. Natl. Acad. Sci. U. S. A* 112, E3067–E3074. <https://10.1073/pnas.1422336112>. [PubMed: 26015580]
- Morales M, Margolis EB, 2017 Ventral tegmental area: Cellular heterogeneity, connectivity and behaviour. *Nat. Rev. Neurosci* 18, 73–85. <https://10.1038/nrn.2016.165>. [PubMed: 28053327]
- Morales M, Root DH, 2014 Glutamate neurons within the midbrain dopamine regions. *Neuroscience* 282, 60–68. <https://10.1016/j.neuroscience.2014.05.032>. [PubMed: 24875175]
- Morin N, Jourdain VA, Di Paolo T, 2014 Modeling dyskinesia in animal models of parkinson disease. *Exp. Neurol* 256, 105–116. <https://10.1016/j.expneurol.2013.01.024>. [PubMed: 23360802]
- Moss J, Bolam JP, 2008 A dopaminergic axon lattice in the striatum and its relationship with cortical and thalamic terminals. *J. Neurosci* 28, 11221–11230. <https://10.1523/JNEUROSCI.2780-08.2008>. [PubMed: 18971464]
- Munoz A, Lopez-Lopez A, Labandeira CM, Labandeira-Garcia JL, 2020 Interactions between the serotonergic and other neurotransmitter systems in the basal ganglia: Role in parkinson's disease and adverse effects of l-dopa. *Front. Neuroanat* 14, 26 <https://10.3389/fnana.2020.00026>. [PubMed: 32581728]
- Neely MD, Schmidt DE, Deutch AY, 2007 Cortical regulation of dopamine depletion-induced dendritic spine loss in striatal medium spiny neurons. *Neuroscience* 149, 457–464. <https://10.1016/j.neuroscience.2007.06.044>. [PubMed: 17888581]
- New JS, 1990 The discovery and development of buspirone: a new approach to the treatment of anxiety. *Med. Res. Rev* 10, 283–326. <https://10.1002/med.2610100302>. [PubMed: 2196403]
- Ninan I, Bath KG, et al., 2010 The bdnf val66met polymorphism impairs nmda receptor-dependent synaptic plasticity in the hippocampus. *J. Neurosci* 30, 8866–8870. <https://10.1523/JNEUROSCI.1405-10.2010>. [PubMed: 20592208]
- Numakawa T, Odaka H, Adachi N, 2017 Actions of brain-derived neurotrophic factor and glucocorticoid stress in neurogenesis. *Int. J. Mol. Sci* 18 <https://10.3390/ijms18112312>.
- Olanow C, Bartus RT, et al., 2015 Gene delivery of neurturin to putamen and substantia nigra in parkinson disease: a double-blind, randomized, controlled trial. *Ann. Neurol* 78, 248–257. <https://10.1002/ana.24436>. [PubMed: 26061140]
- Olanow CW, Goetz CG, et al., 2003 A double-blind controlled trial of bilateral fetal nigral transplantation in parkinson's disease. *Ann. Neurol* 54, 403–414. <https://10.1002/ana.10720>. [PubMed: 12953276]
- Olanow CW, Kordower JH, Lang AE, Obeso JA, 2009 Dopaminergic transplantation for parkinson's disease: current status and future prospects. *Ann. Neurol* 66, 591–596. <https://10.1002/ana.21778>. [PubMed: 19938101]
- Orefice LL, Shih CC, Xu H, Waterhouse EG, Xu B, 2016 Control of spine maturation and pruning through probdnf synthesized and released in dendrites. *Mol. Cell. Neurosci* 71, 66–79. <https://10.1016/j.mcn.2015.12.010>. [PubMed: 26705735]
- Park H, Poo MM, 2013 Neurotrophin regulation of neural circuit development and function. *Nat. Rev. Neurosci* 14, 7–23. <https://10.1038/nrn3379>. [PubMed: 23254191]
- Patterson SL, Abel T, et al., 1996 Recombinant bdnf rescues deficits in basal synaptic transmission and hippocampal ltp in bdnf knockout mice. *Neuron* 16, 1137–1145. [https://10.1016/s0896-6273\(00\)80140-3](https://10.1016/s0896-6273(00)80140-3). [PubMed: 8663990]
- Pattwell SS, Bath KG, et al., 2012 The bdnf val66met polymorphism impairs synaptic transmission and plasticity in the infralimbic medial prefrontal cortex. *J. Neurosci* 32, 2410–2421. <https://10.1523/JNEUROSCI.5205-11.2012>. [PubMed: 22396415]
- Petryshen TL, Sabeti PC, et al., 2010 Population genetic study of the brain-derived neurotrophic factor (bdnf) gene. *Mol. Psychiatry* 15, 810–815. <https://10.1038/mp.2009.24>. [PubMed: 19255578]

- Piccini P, Pavese N, et al., 2005 Factors affecting the clinical outcome after neural transplantation in parkinson's disease. *Brain* 128, 2977–2986. <https://10.1093/brain/awh649>. [PubMed: 16246865]
- Pickel VM, Beckley SC, Joh TH, Reis DJ, 1981 Ultrastructural immunocytochemical localization of tyrosine hydroxylase in the neostriatum. *Brain Res.* 225, 373–385. [https://10.1016/0006-8993\(81\)90843-x](https://10.1016/0006-8993(81)90843-x). [PubMed: 6118197]
- Politis M, Wu K, et al., 2010 Serotonergic neurons mediate dyskinesia side effects in parkinson's patients with neural transplants. *Sci. Transl. Med* 2, 38ra46–38ra46. <https://10.1126/scitranslmed.3000976>.
- Politis M, Oertel WH, et al., 2011 Graft-induced dyskinesias in parkinson's disease: high striatal serotonin/dopamine transporter ratio. *Mov. Disord* 26, 1997–2003. <https://10.1002/mds.23743>. [PubMed: 21611977]
- Prakash N, Wurst W, 2006 Development of dopaminergic neurons in the mammalian brain. *Cell. Mol. Life Sci* 63, 187–206. <https://10.1007/s00018-005-5387-6>. [PubMed: 16389456]
- Qin L, Jing D, et al., 2014 An adaptive role for bdnf val66met polymorphism in motor recovery in chronic stroke. *J. Neurosci* 34, 2493–2502. <https://10.1523/JNEUROSCI.4140-13.2014>. [PubMed: 24523540]
- Rauskolb S, Zagrebelsky M, et al., 2010 Global deprivation of brain-derived neurotrophic factor in the cns reveals an area-specific requirement for dendritic growth. *J. Neurosci* 30, 1739–1749. <https://10.1523/JNEUROSCI.5100-09.2010>. [PubMed: 20130183]
- Razgado-Hernandez LF, Espadas-Alvarez AJ, et al., 2015 The transfection of bdnf to dopamine neurons potentiates the effect of dopamine d3 receptor agonist recovering the striatal innervation, dendritic spines and motor behavior in an aged rat model of parkinson's disease. *PLoS One* 10, e0117391 <https://10.1371/journal.pone.0117391>. [PubMed: 25693197]
- Rylander D, Parent M, et al., 2010 Maladaptive plasticity of serotonin axon terminals in levodopa-induced dyskinesia. *Ann. Neurol* 68, 619–628. <https://10.1002/ana.22097>. [PubMed: 20882603]
- Saylor AJ, Meredith GE, Vercillo MS, Zahm DS, McGinty JF, 2006 Bdnf heterozygous mice demonstrate age-related changes in striatal and nigral gene expression. *Exp. Neurol* 199, 362–372. <https://10.1016/j.expneurol.2006.01.004>. [PubMed: 16478623]
- Segal M, Vlachos A, Korkotian E, 2010 The spine apparatus, synaptopodin, and dendritic spine plasticity. *Neuroscientist* 16, 125–131. <https://10.1177/1073858409355829>. [PubMed: 20400711]
- Sellnow RC, Newman JH, et al., 2019 Regulation of dopamine neurotransmission from serotonergic neurons by ectopic expression of the dopamine d2 autoreceptor blocks levodopa-induced dyskinesia. *Acta Neuropathol Commun* 7, 8 <https://10.1186/s40478-018-0653-7>. [PubMed: 30646956]
- Shin E, Garcia J, Winkler C, Bjorklund A, Carta M, 2012a Serotonergic and dopaminergic mechanisms in graft-induced dyskinesia in a rat model of parkinson's disease. *Neurobiol. Dis* 47, 393–406. <https://10.1016/j.nbd.2012.03.038>. [PubMed: 22579773]
- Shin E, Tronci E, Carta M, 2012b Role of serotonin neurons in l-dopa- and graft-induced dyskinesia in a rat model of parkinson's disease. *Parkinsons Dis* 2012, 370190 <https://10.1155/2012/370190>. [PubMed: 22762012]
- Shin E, Lisci C, et al., 2014 The anti-dyskinetic effect of dopamine receptor blockade is enhanced in parkinsonian rats following dopamine neuron transplantation. *Neurobiol. Dis* 62, 233–240. <https://10.1016/j.nbd.2013.09.021>. [PubMed: 24135006]
- Sieber BA, Landis S, et al., 2014 Prioritized research recommendations from the national institute of neurological disorders and stroke parkinson's disease 2014 conference. *Ann. Neurol* 76, 469–472. <https://10.1002/ana.24261>. [PubMed: 25164235]
- Smith GA, Breger LS, Lane EL, Dunnett SB, 2012a Pharmacological modulation of amphetamine-induced dyskinesia in transplanted hemi-parkinsonian rats. *Neuropharmacology* 63, 818–828. <https://10.1016/j.neuropharm.2012.06.011>. [PubMed: 22722025]
- Smith GA, Heuer A, et al., 2012b Amphetamine-induced dyskinesia in the transplanted hemi-parkinsonian mouse. *J. Parkinsons Dis* 2, 107–113. <https://10.3233/JPD-2012-12102>. [PubMed: 23933747]

- Soderstrom KE, Meredith G, et al., 2008 The synaptic impact of the host immune response in a parkinsonian allograft rat model: influence on graft-derived aberrant behaviors. *Neurobiol. Dis* 32, 229–242. <https://10.1016/j.nbd.2008.06.018>. [PubMed: 18672063]
- Soderstrom KE, O'Malley JA, et al., 2010 Impact of dendritic spine preservation in medium spiny neurons on dopamine graft efficacy and the expression of dyskinesias in parkinsonian rats. *Eur. J. Neurosci* 31, 478–490. <https://10.1111/j.1460-9568.2010.07077.x>. [PubMed: 20105237]
- Sortwell CE, Auinger Peggy, Goudreau John L., Pickut Barbara, Berryhill Brian, Hacker Mallory L., Charles David, Lipton Jack W., Cole-Strauss Allyson, Elm Jordan J., Fischer D. Luke, 2017 Specific bdnf variants are associated with suboptimal response to levodopa but not to other dopaminergic medications or deep brain stimulation in parkinson's disease. *Mov. Disord* 32 (Suppl. 2).
- Steece-Collier K, Collier TJ, Sladek CD, Sladek JR Jr., 1990 Chronic levodopa impairs morphological development of grafted embryonic dopamine neurons. *Exp. Neurol* 110, 201–208. [https://10.1016/0014-4886\(90\)90031-m](https://10.1016/0014-4886(90)90031-m). [PubMed: 2226699]
- Steece-Collier K, Collier TJ, et al., 2003 Embryonic mesencephalic grafts increase levodopa-induced forelimb hyperkinesia in parkinsonian rats. *Mov. Disord* 18, 1442–1454. <https://10.1002/mds.10588>. [PubMed: 14673880]
- Steece-Collier K, Rademacher DJ, Soderstrom K, 2012 Anatomy of graft-induced dyskinesias: Circuit remodeling in the parkinsonian striatum. *Basal Ganglia* 2, 15–30. <https://10.1016/j.baga.2012.01.002>. [PubMed: 22712056]
- Steece-Collier K, Stancati JA, et al., 2019 Genetic silencing of striatal cav1.3 prevents and ameliorates levodopa dyskinesia. *Mov. Disord* 34, 697–707. <https://10.1002/mds.27695>. [PubMed: 31002755]
- Steece-Collier K, Collier TJ, et al., 2020 Striatal nurr1, but not fosb expression links a levodopa-induced dyskinesia phenotype to genotype in fisher 344 vs. Lewis hemiparkinsonian rats. *Exp. Neurol* 330, 113327 <https://10.1016/j.expneurol.2020.113327>. [PubMed: 32387398]
- Stephens B, Mueller AJ, et al., 2005 Evidence of a breakdown of corticostriatal connections in parkinson's disease. *Neuroscience* 132, 741–754. <https://10.1016/j.neuroscience.2005.01.007>. [PubMed: 15837135]
- Stoker TB, Blair NF, Barker RA, 2017 Neural grafting for parkinson's disease: Challenges and prospects. *Neural Regen. Res* 12, 389–392. <https://10.4103/1673-5374.202935>. [PubMed: 28469646]
- Tenenbaum L, Humbert-Claude M, 2017 Glial cell line-derived neurotrophic factor gene delivery in parkinson's disease: a delicate balance between neuroprotection, trophic effects, and unwanted compensatory mechanisms. *Front. Neuroanat* 11, 29 <https://10.3389/fnana.2017.00029>. [PubMed: 28442998]
- Teng HK, Teng KK, et al., 2005 Probdnf induces neuronal apoptosis via activation of a receptor complex of p75ntr and sortilin. *J. Neurosci* 25, 5455–5463. <https://10.1523/JNEUROSCI.5123-04.2005>. [PubMed: 15930396]
- Towns CR, 2017 The science and ethics of cell-based therapies for parkinson's disease. *Parkinsonism Relat. Disord* 34, 1–6. <https://10.1016/j.parkreldis.2016.10.012>. [PubMed: 28341222]
- Tronci E, Fidalgo C, Carta M, 2015 Foetal cell transplantation for parkinson's disease: Focus on graft-induced dyskinesia. *Parkinsons Dis* 2015, 563820 <https://10.1155/2015/563820>. [PubMed: 26881178]
- Villalba RM, Lee H, Smith Y, 2009 Dopaminergic denervation and spine loss in the striatum of mptp-treated monkeys. *Exp. Neurol* 215, 220–227. <https://10.1016/j.expneurol.2008.09.025>. [PubMed: 18977221]
- Vlachos A, Korkotian E, et al., 2009 Synaptopodin regulates plasticity of dendritic spines in hippocampal neurons. *J. Neurosci* 29, 1017–1033. <https://10.1523/JNEUROSCI.5528-08.2009>. [PubMed: 19176811]
- Woo NH, Teng HK, et al., 2005 Activation of p75ntr by probdnf facilitates hippocampal long-term depression. *Nat. Neurosci* 8, 1069–1077. <https://10.1038/nn1510>. [PubMed: 16025106]

- Wu LL, Fan Y, Li S, Li XJ, Zhou XF, 2010 Huntingtin-associated protein-1 interacts with pro-brain-derived neurotrophic factor and mediates its transport and release. *J. Biol. Chem* 285, 5614–5623. <https://10.1074/jbc.M109.073197>. [PubMed: 19996106]
- Xie Y, Hayden MR, Xu B, 2010 Bdnf overexpression in the forebrain rescues huntington's disease phenotypes in yac128 mice. *J. Neurosci* 30, 14708–14718. <https://10.1523/JNEUROSCI.1637-10.2010>. [PubMed: 21048129]
- Yurek DM, Lu W, Hipkens S, Wiegand SJ, 1996 Bdnf enhances the functional reinnervation of the striatum by grafted fetal dopamine neurons. *Exp. Neurol* 137, 105–118. <https://10.1006/exnr.1996.0011>. [PubMed: 8566202]
- Yurek DM, Hipkens SB, Wiegand SJ, Altar CA, 1998 Optimal effectiveness of bdnf for fetal nigral transplants coincides with the ontogenic appearance of bdnf in the striatum. *J. Neurosci* 18, 6040–6047. [PubMed: 9671688]
- Zagrebelsky M, Korte M, 2014 Form follows function: Bdnf and its involvement in sculpting the function and structure of synapses. *Neuropharmacology* 76 (Pt C), 628–638. <https://10.1016/j.neuropharm.2013.05.029>. [PubMed: 23752094]
- Zaja-Milatovic S, Milatovic D, et al., 2005 Dendritic degeneration in neostriatal medium spiny neurons in parkinson disease. *Neurology* 64, 545–547. <https://10.1212/01.WNL.0000150591.33787.A4>. [PubMed: 15699393]
- Zanin JP, Unsain N, Anastasia A, 2017 Growth factors and hormones pro-peptides: the unexpected adventures of the bdnf prodomain. *J. Neurochem* 141, 330–340. <https://10.1111/jnc.13993>. [PubMed: 28218971]
- Zhang Y, Meredith GE, et al., 2013 Aberrant restoration of spines and their synapses in l-dopa-induced dyskinesia: Involvement of corticostriatal but not thalamostriatal synapses. *J. Neurosci* 33, 11655–11667. <https://10.1523/JNEUROSCI.0288-13.2013>. [PubMed: 23843533]
- Zhou J, Bradford HF, Stern GM, 1997 Influence of bdnf on the expression of the dopaminergic phenotype of tissue used for brain transplants. *Brain Res. Dev. Brain Res* 100, 43–51. [PubMed: 9174245]
- Zuccato C, Cattaneo E, 2007 Role of brain-derived neurotrophic factor in huntington's disease. *Prog. Neurobiol* 81, 294–330. <https://10.1016/j.pneurobio.2007.01.003>. [PubMed: 17379385]

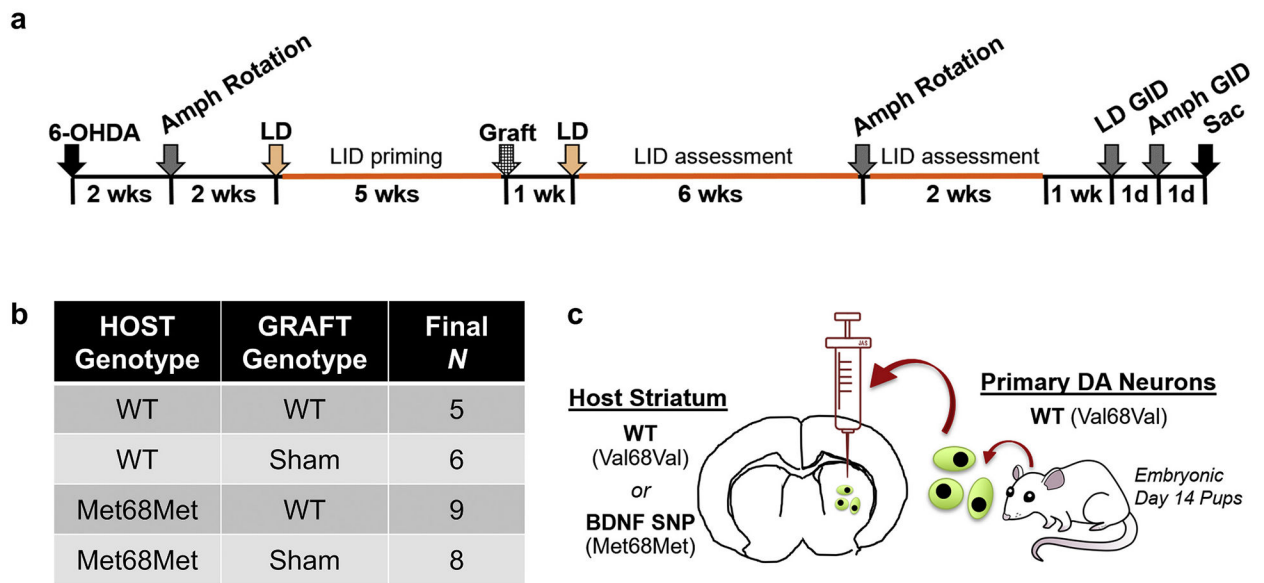


Fig. 1.

Experimental design. **a** Experimental timeline of surgical procedures, behavioral evaluation, and drug treatment. **b** Experimental groups and final group size “*N*” upon completion of the study. **c** Schematic depicting the design of experiments. Ventral mesencephalic tissue was dissected from wild-type embryonic day 14 Sprague-Dawley rat pups, dissociated, then transplanted into wild-type Val68Val and homozygous Met68Met rats. Abbreviations: 6-OHDA = 6-hydroxydopamine, Amph rotation = amphetamine rotation behavioral assessment, LD = levodopa, LID = levodopa-induced dyskinesia, GID = graft-induced dyskinesia, LD GID = levodopa-mediated GID assessment, Amph GID = amphetamine-mediated GID assessment, sac = sacrifice, WT = wild-type, BDNF = brain-derived neurotrophic factor, SNP = single nucleotide polymorphism, DA = dopamine

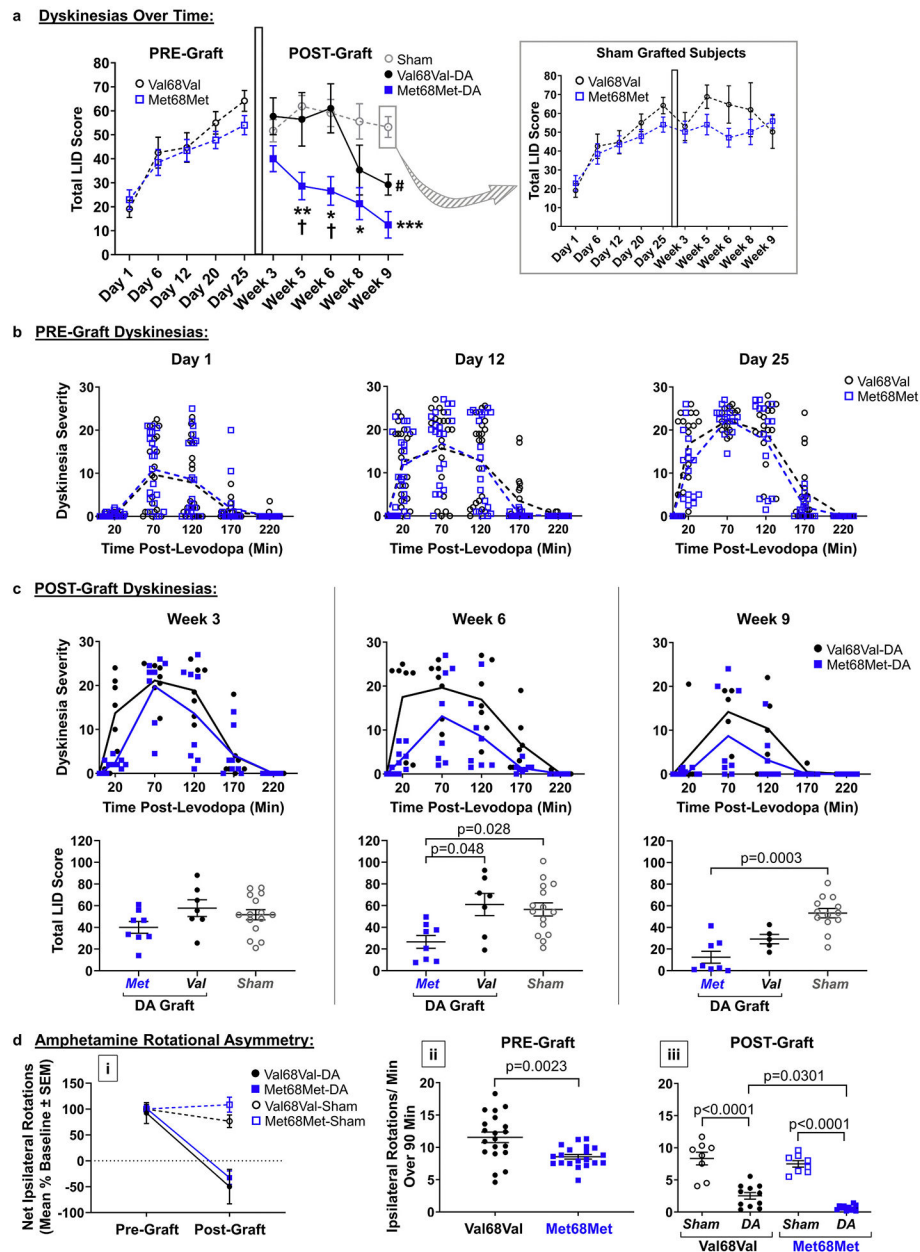


Fig. 2. Behavioral measures of graft functional efficacy. a Total LID score (primary behavioral endpoint) for Val68Val and Met68Met rats throughout levodopa priming (pre-graft period) and for 9 weeks post-engraftment. Dyskinesia severity scores were not significantly different between genotypes in sham grafted rats; thus, sham subjects were combined into one group post-graft. Inset graph depicts total dyskinesia score over time for sham grafted subjects, separated by genotype. Statistics: Non-parametric Kruskal-Wallis test with Dunn's multiple comparisons test at each time point. Week 5: ** $p = 0.0015$ Met68Met-DA vs Sham, † $p = 0.0302$ Met68Met-DA vs Val68Val-DA; Week 6: * $p = 0.0284$ Met68Met-DA vs Sham, † $p = 0.0475$ Met68Met-DA vs Val68Val-DA; Week 8: * $p = 0.0198$ Met68Met-DA vs Sham; Week 9: *** $p = 0.0003$ Met68Met-DA vs Sham. Sham groups were not significantly

different at any of the post-graft time points ($p = 0.12$ for all time points post-graft). b Pre-graft LID severity time course showing individual animal responses during levodopa priming days 1, 12, and 25. Rats were rated at 20, 70, 120, 170, and 220 mins post-levodopa each day. c LID severity time course and total LID scores showing individual animal responses at weeks 3, 6, and 9 post-engraftment. Non-parametric Kruskal-Wallis test with Dunn's multiple comparisons test at each time point. d Amphetamine rotational asymmetry (secondary behavioral endpoint), measured at 7 weeks pre-graft and 7 weeks post-graft. Data are expressed as net ipsilateral rotations (i) and ipsilateral rotations per min over 90 mins (ii–iii). Unpaired t -test with Welch's correction (ii) and one-way ANOVA with Šídák's post-hoc test (iii). Abbreviations: LID = levodopa-induced dyskinesia, DA = dopamine graft, CCW = counterclockwise

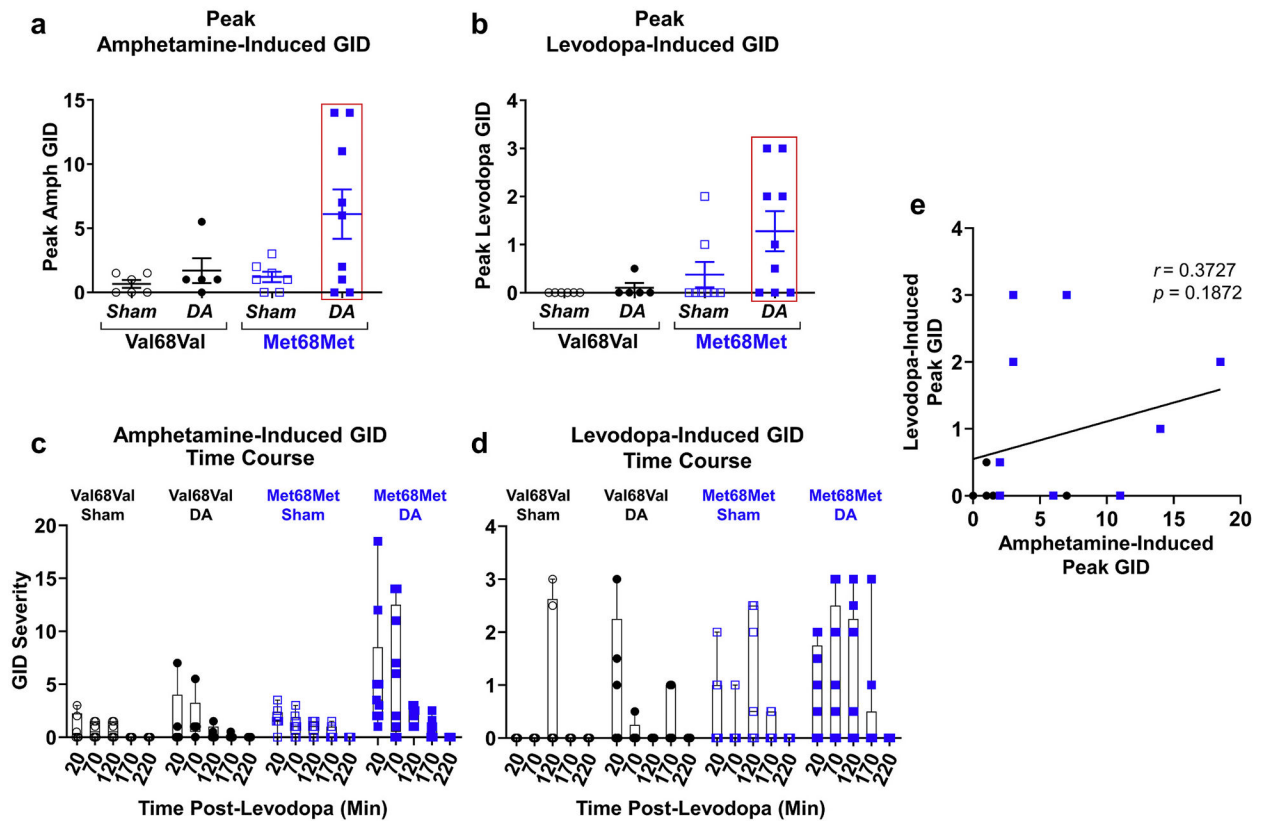


Fig. 3. Behavioral measures of graft dysfunction. a,b Peak amphetamine-induced (a) and levodopa-induced (b) GID severity score at week 10 post-engraftment. Non-parametric Kruskal-Wallis test with Dunn's post-hoc comparisons. c,d Time course of amphetamine-mediated (c) and levodopa-mediated (d) GID behavior at week 10 post-engraftment. e Spearman correlation between amphetamine-mediated peak GID behavior and levodopa-mediated peak GID behavior. Abbreviations: GID = graft-induced dyskinesia, Amph = amphetamine, DA = dopamine graft

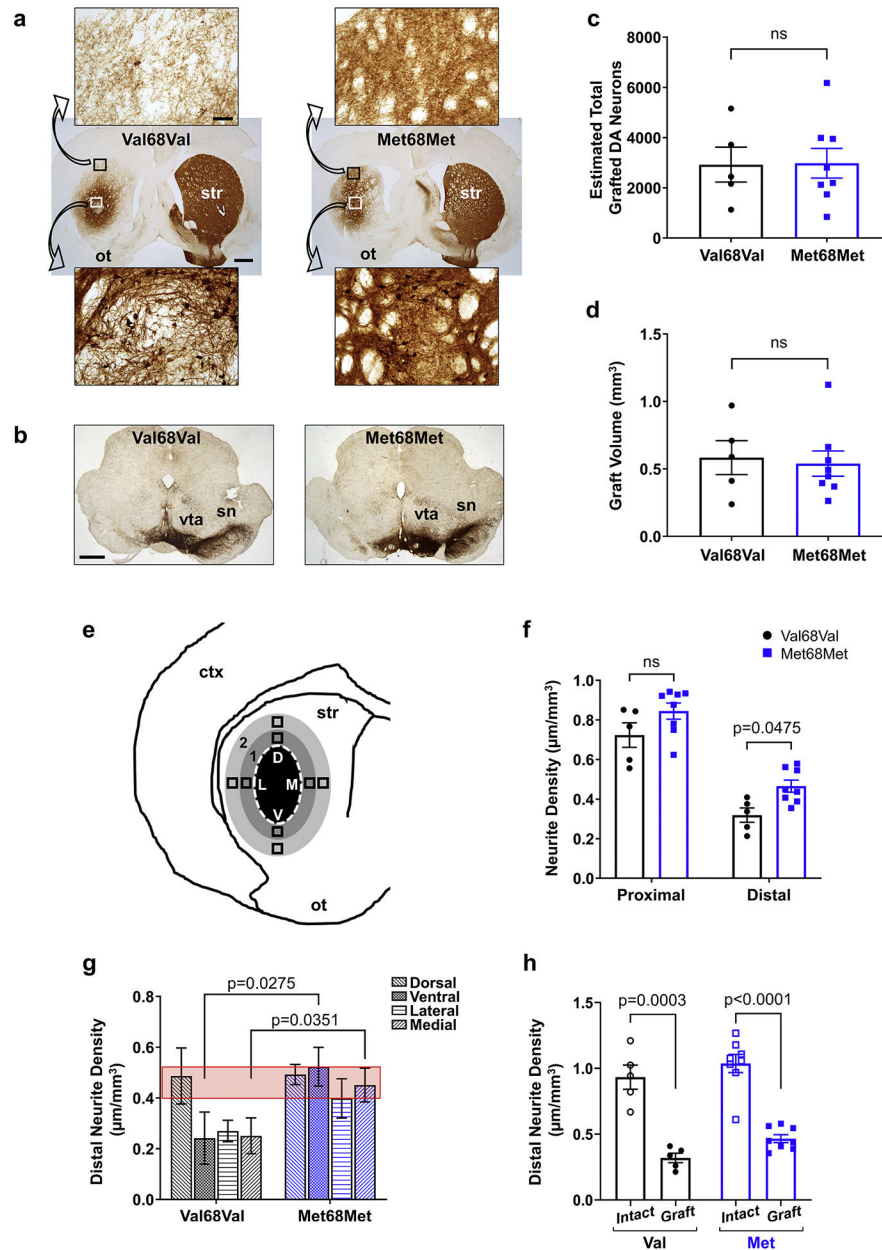


Fig. 4. Graft histology in parkinsonian striatum of Met68Met rats and their wild-type (Val68Val) counterparts. **a** Representative micrographs of THir striatum demonstrating more extensive grafted DA neurite outgrowth in Met68Met host striatum. Scale bars = 100 μm (10x micrographs), 1000 μm (1x micrographs). **b** Corresponding THir nigral tissue sections showing near-complete depletion of host SNc DA neurons in the lesioned hemisphere. Scale bar = 1000 μm . **c** Stereologically estimated total number of grafted DA neurons. Mean \pm SEM. Unpaired t -test. **d** Stereologically estimated total graft volume. Mean \pm SEM. Unpaired t -test. **e** Schematic illustrating fields of view used for analysis of grafted DA neurite outgrowth. Proximal and distal regions are denoted by “1” and “2,” respectively. **f** Average grafted DA neurite density proximal and distal to the graft border. Mean \pm SEM.

Two-way repeated measures ANOVA with Šídák's post-hoc test. g Comparison of distal grafted DA neurite outgrowth separated into regions surrounding the graft. Mean \pm SEM. Unpaired *t*-tests and mixed-effects model. *Red bar* indicates maximum and minimum neurite density means for Met68Met subjects. h Distal grafted DA neurite density compared with endogenous DA innervation of intact contralateral striatum. Mean \pm SEM. Two-way repeated measures ANOVA with Šídák's post-hoc test. Abbreviations: THir = tyrosine hydroxylase immunoreactive, str = striatum, ot = olfactory tubercle, vta = ventral tegmental area, sn = substantia nigra, ctx = cortex, D = dorsal, M = medial, V = ventral, L = lateral, 1 = proximal zone, 2 = distal zone, ns = not significant

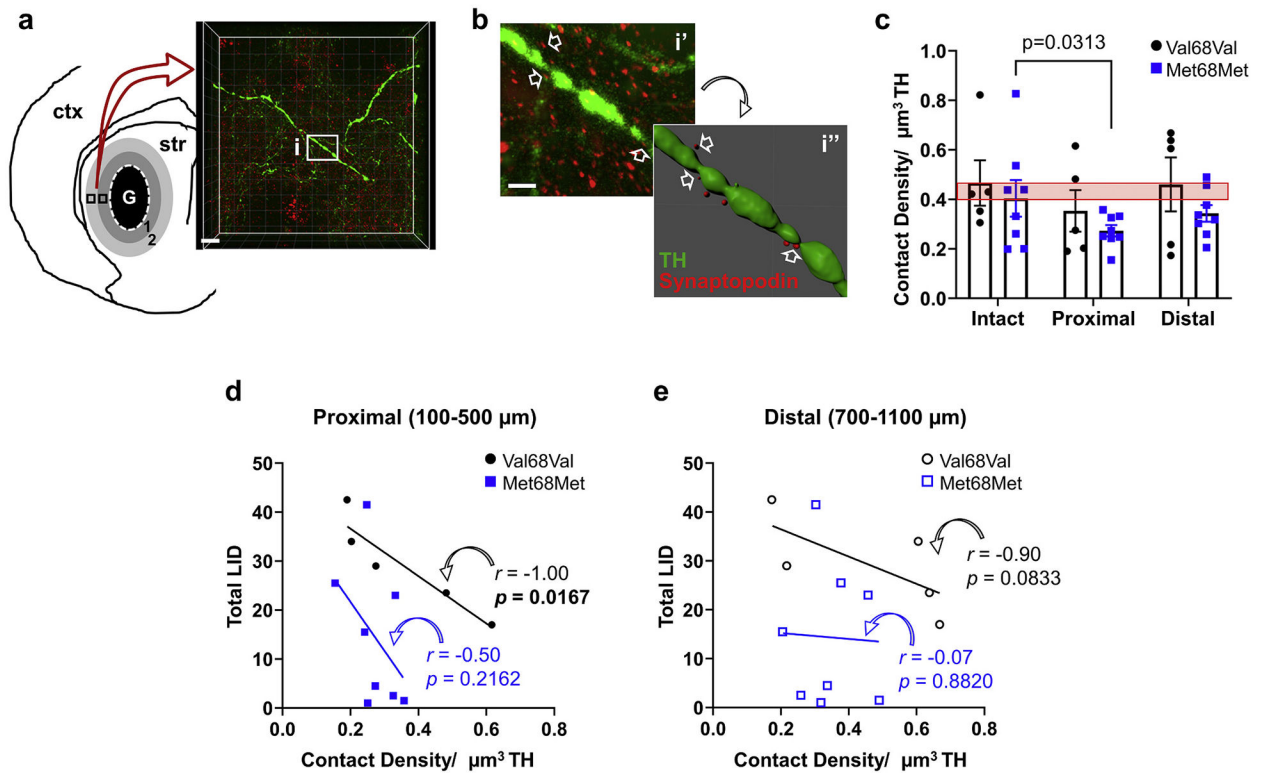
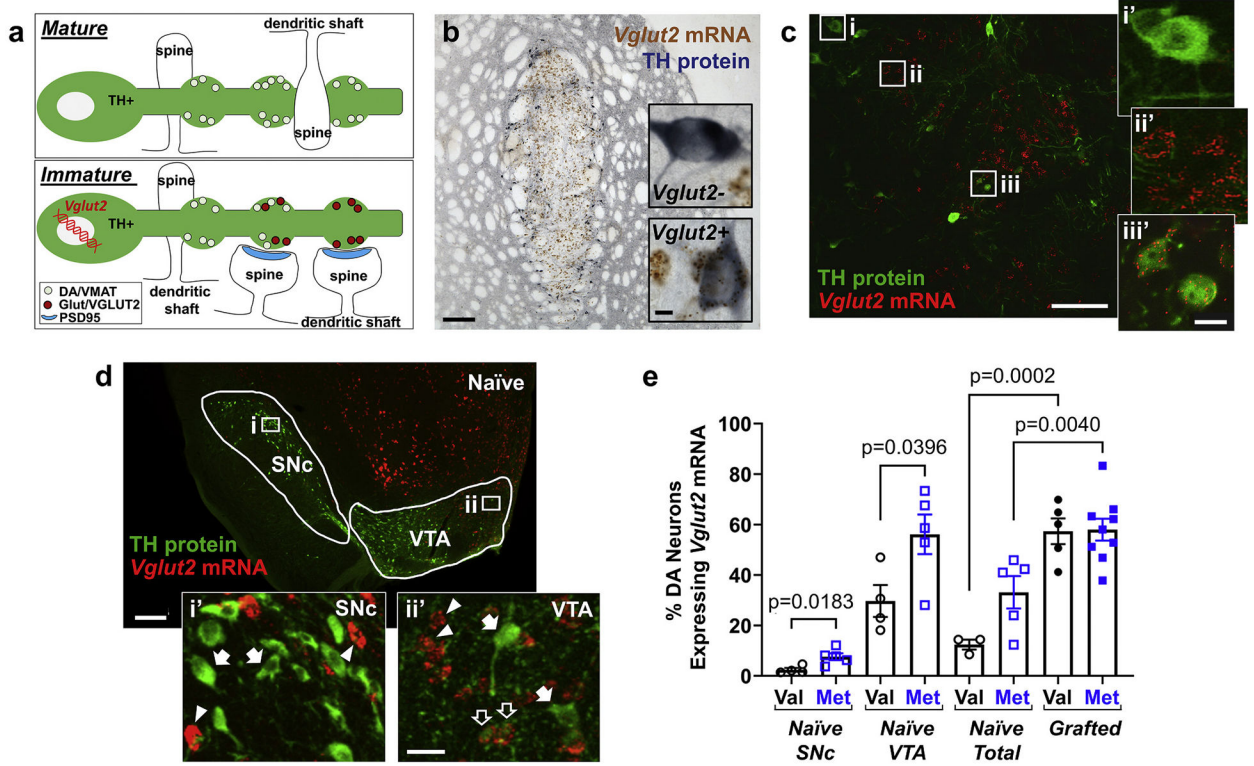


Fig. 5. Impact of Met allele on graft (TH) connectivity with host MSN spines (synaptopodin). **a** Schematic representation of regions relative to the graft in which confocal images were acquired (left), and representative 3D confocal z-stack of grafted DA neurites in tissue stained for TH and synaptopodin (right). Scale bar = 10 μm . **b** (*i'*) Increased magnification of micrograph in panel (a), and (*i''*) Imaris® 3D reconstruction of DA fiber denoted by (*i*) in panel (a). Scale bar = 1 μm . **c** Comparison of TH-synaptopodin contact density normalized to TH surface volume. Mean \pm SEM. Two-way mixed-effects model with repeated measures, followed by Šídák's and Dunnett's post-hoc tests. *Red bar* indicates maximum and minimum contact density means in the intact striatum. **d** Spearman correlation between *proximal* TH-synaptopodin contact density and total LID severity score at 9 wks post-engraftment. **e** Spearman correlation between *distal* TH-synaptopodin contact density and total LID severity score at 9 wks post-engraftment. Abbreviations: ctx = cortex, str = striatum, 1 = proximal zone, 2 = distal zone

**Fig. 6.**

Vglut2 mRNA expression in DA neurons grafted into parkinsonian striatum. **a** Schematic depicting normal mature vs immature DA neuron phenotype, based on data from (El Mestikawy et al., 2011). **b,c** *Vglut2* mRNA expression in TH⁺ grafted DA neurons and unidentified grafted TH-negative cells. Cells denoted by (i-iii) in panel (c) are shown with increased magnification in (i'-iii'). Scale bars = 250 μ m in panel (b) and 5 μ m for insets in this panel; 100 μ m in panel (c), or 10 μ m for insets in this panel. **d** *Vglut2* mRNA in DA neurons of the naïve adult rat midbrain. DA neurons of the substantia nigra (i) and ventral tegmental area (ii) are shown with increased magnification in (i') and (ii'), respectively. *Vglut2*-negative DA neurons are indicated by solid arrows in (i') and (ii'), whereas solid arrowheads indicate cells containing *Vglut2* mRNA only, and unfilled arrows indicate cells containing colocalized TH-*Vglut2*. Scale bars = 300 μ m for panel (d), and 30 μ m for i' and ii'. **e** Percentage of DA neurons expressing *Vglut2* mRNA in naïve adult rat midbrain and grafted, parkinsonian striatum. NOTE: Grafted DA neurons are from wild-type donors. Mean \pm SEM. Two-way ANOVA with Šídák's post-hoc test (Naïve Total and Grafted); unpaired *t*-tests (naïve SNc and naïve VTA). Abbreviations: DA = dopamine, VMAT = vesicular monoamine transporter, Glut = glutamate, VGLUT2 = vesicular glutamate transporter 2, TH = tyrosine hydroxylase, SNc = substantia nigra pars compacta, VTA = ventral tegmental area

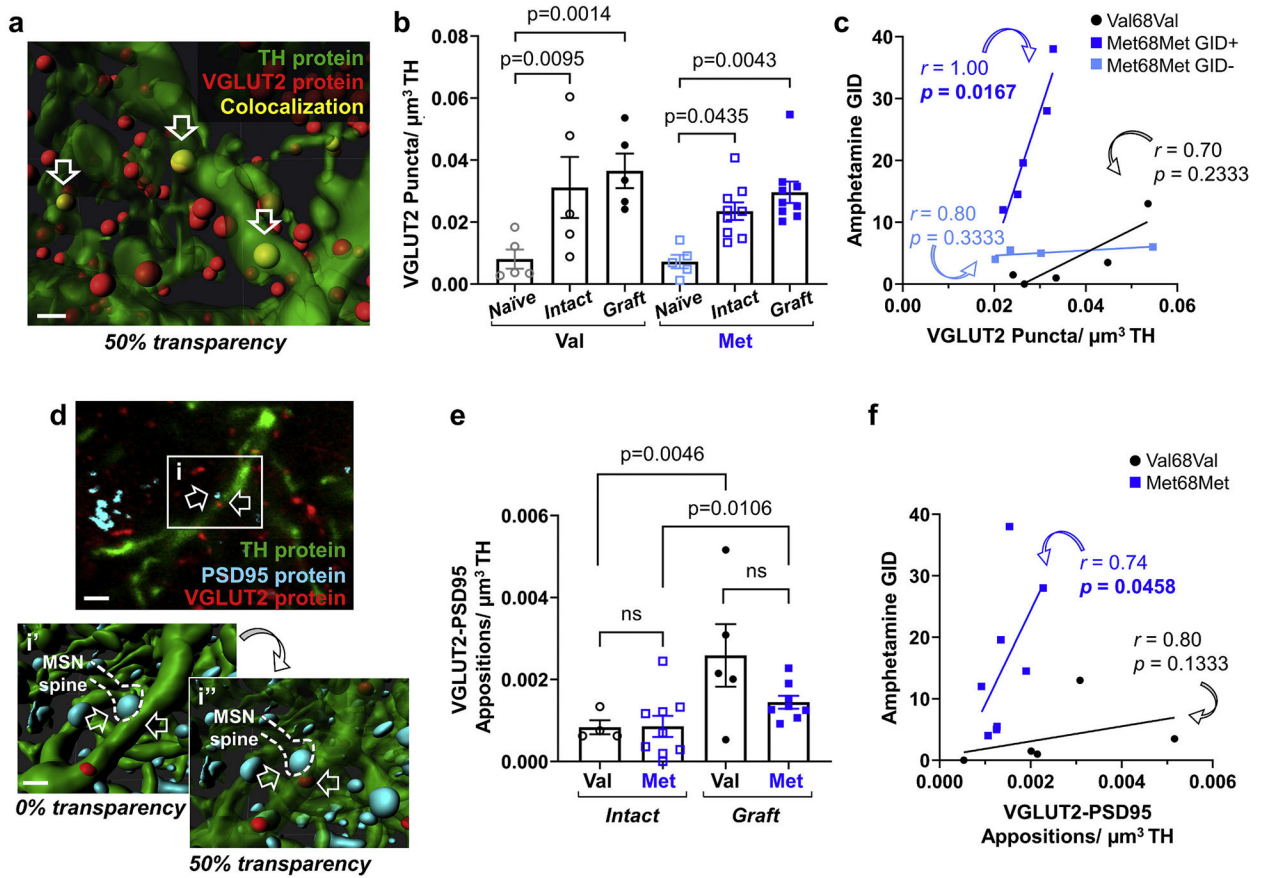


Fig. 7.

VGLUT2 protein expression in THir DA fibers grafted into parkinsonian striatum. a Computer generated Imaris® 3D reconstruction of confocal z-stack depicting VGLUT2 colocalization within grafted DA neurites. The advanced Imaris® algorithms allow visualization of fine structures (i.e., vesicles) inside cellular elements (i.e., neurites), and allows the cellular element to be visualized at varying levels of transparency (i.e., 50% shown here) to allow visualization of internal elements. Scale bar = 1 μm . b Quantification of VGLUT2 protein located within THir DA fibers, normalized to TH surface volume. TH-VGLUT2 colocalization in the striatum of naïve rats was compared with grafted DA fibers in the parkinsonian striatum and endogenous DA fibers in the intact striatum contralateral to the lesion. Mean \pm SEM. Two-way ANOVAs with Tukey's post-hoc test. c Spearman correlation between TH-VGLUT2 colocalization in grafted DA neurites and total amphetamine-mediated GID score at 10 wks post-engraftment. d Confocal micrograph indicating synaptic apposition ($\approx 0.6 \mu\text{m}$) between VGLUT2 protein located inside a grafted DA neurite (indicated by open arrow on the right) and PSD95 located adjacent to the DA neurite (indicated by open arrow on the left). The presumed synapse (i) is shown with increased magnification using Imaris® 3D imaging in (i') and (i''). Scale bars = 2 μm (confocal micrograph), 1 μm (Imaris® 3D reconstructions). % transparency indicates that applied to TH fibers. e Quantification of presumed excitatory VGLUT2-PSD95 synapses made by DA neurites in the grafted striatum and intact contralateral striatum, normalized to TH surface volume. Mean \pm SEM. Mixed-effects model with Šidák's post-hoc test. f

Spearman correlation between presumed excitatory VGLUT2-PSD95 synapses made by DA neurites and total amphetamine-mediated GID score at 10 wks post-engraftment. Note that one statistical outlier was removed from the Met68Met group. Abbreviations: VGLUT2 = vesicular glutamate transporter 2, PSD95 = postsynaptic density protein 95, TH = tyrosine hydroxylase, MSN = medium spiny neuron, ns = not significant

Author Manuscript

Author Manuscript

Author Manuscript

Author Manuscript

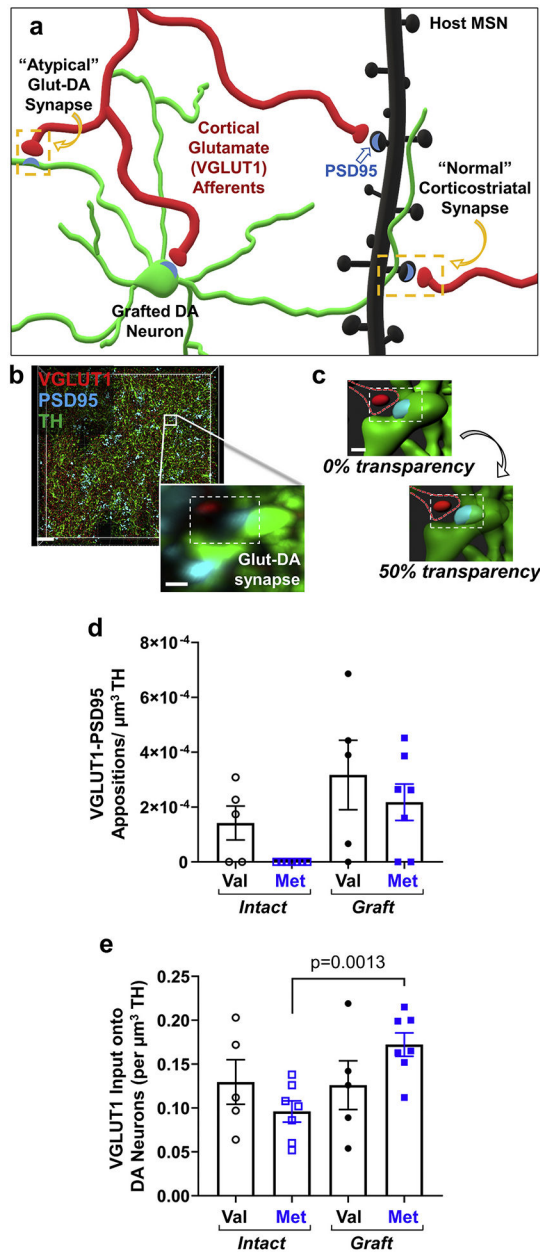


Fig. 8. Excitatory corticostriatal (VGLUT1) synaptic input onto grafted DA neurons. **a** Schematic depicting "normal" corticostriatal synapse with modulatory DA input (right side of diagram), and "atypical" excitatory glutamatergic synapse onto grafted DA neurons (left side of diagram). **b** Representative confocal z-stack of tissue stained for VGLUT1, PSD95, and TH proteins. Scale bar = 10 μm . Inset: Increased magnification of a presumed glutamatergic (VGLUT1) synapse onto PSD95 protein located inside a grafted THir DA fiber (0.6 μm). Inset scale bar = 0.5 μm . **c** Imaris® 3D reconstruction of the inset image in panel (b). % transparency indicates that applied to TH fibers. **d** Quantification of presumed corticostriatal (VGLUT1) synapses with PSD95 located inside grafted DA fibers, normalized to TH surface volume. Mean \pm SEM. Two-way repeated measures ANOVA with Šídák's post-hoc

test. e Quantification of presumed corticostriatal (VGLUT1) synapses onto grafted DA fibers, regardless of PSD95 presence, normalized to TH surface volume. Mean \pm SEM. Two-way repeated measures ANOVA with Šídák's post-hoc test. Abbreviations: PSD95 = postsynaptic density protein 95, VGLUT1 = vesicular glutamate transporter 1, Glut = glutamate, DA = dopamine, TH = tyrosine hydroxylase

Author Manuscript

Author Manuscript

Author Manuscript

Author Manuscript

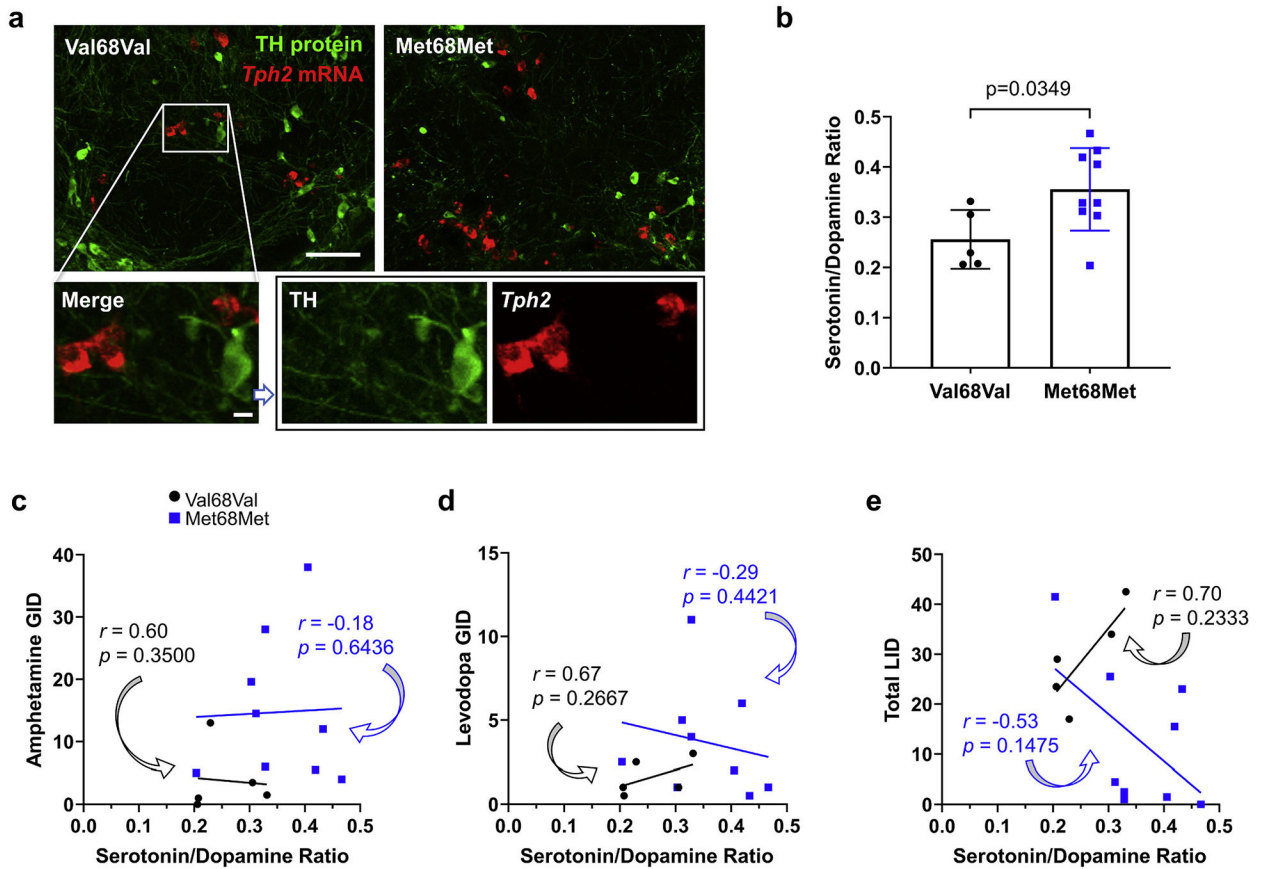
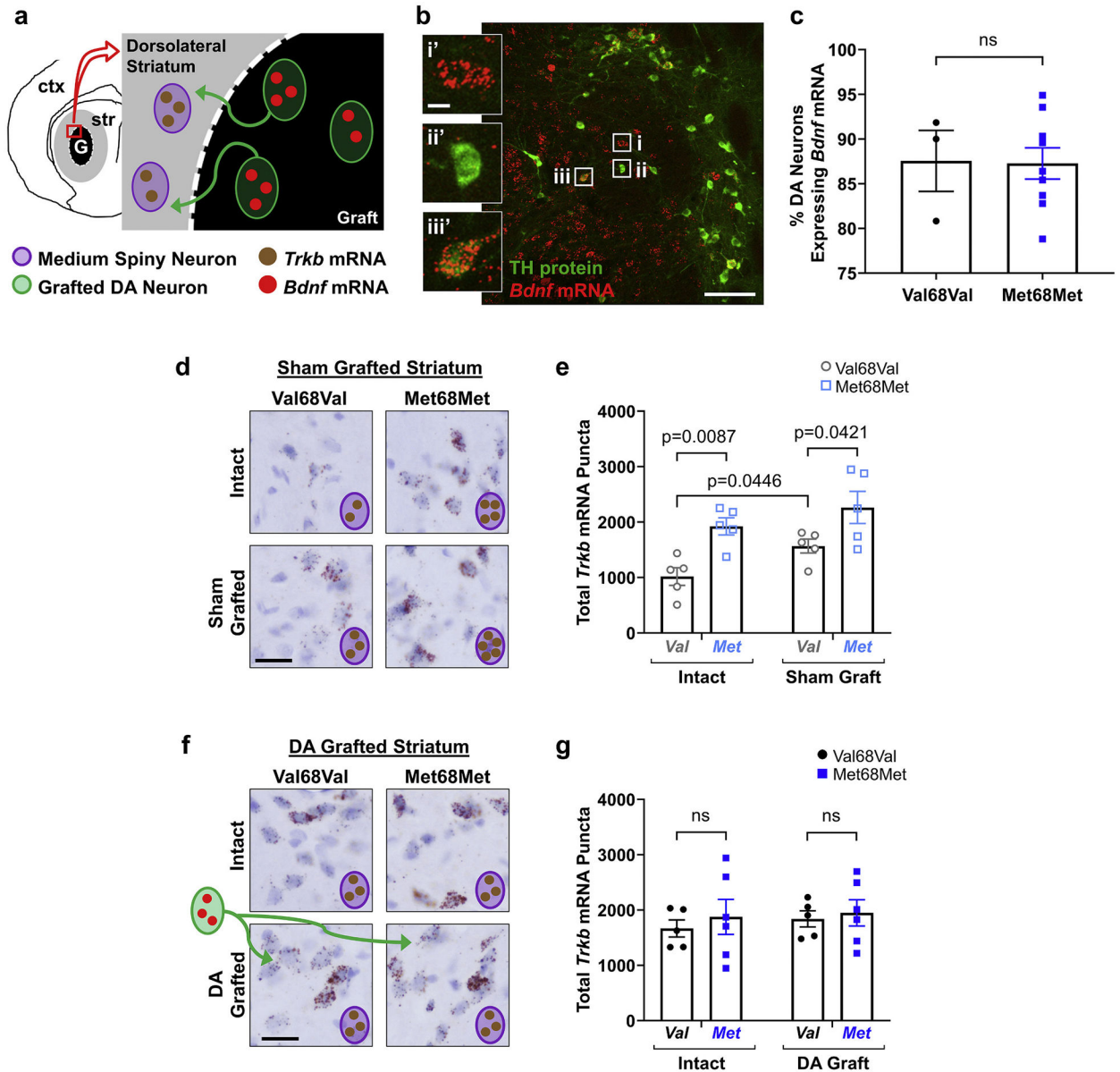


Fig. 9.

Impact of Met allele on presence of serotonin neurons in VM grafts. **a** Confocal micrographs depicting presence of serotonergic neurons in VM grafts from wild-type donors, in Val68Val and Met68Met host striatum. Inset: Increased magnification of DA neurons (THir) and serotonin neurons (*Tph2*-immunoreactive) present in grafted striatum. As shown in these representative images, there was no colocalization of *Tph2* mRNA and TH in VM grafts, and this finding was identical between genotypes. Scale bars = 100 μ m in panel (a), 10 μ m in inset panels. **b** Quantification of grafted serotonin neurons relative to the number of grafted DA neurons. Mean \pm SEM. Unpaired *t*-test. **c** Spearman correlation between the proportion of serotonin neurons relative to DA neurons and total amphetamine-mediated GID score at 10 wks post-engraftment. **d** Spearman correlation between the proportion of serotonin neurons relative to DA neurons and total levodopa-mediated GID score at 10 wks post-engraftment. **e** Spearman correlation between the proportion of serotonin neurons relative to DA neurons and total LID score at 9 wks post-engraftment. Abbreviations: TH = tyrosine hydroxylase, *Tph2* = tryptophan hydroxylase 2

**Fig. 10.**

Impact of Met allele on *Bdnf* mRNA expression in grafted DA neurons and *Trkb* mRNA expression in host striatum. a Schematic illustrating *Trkb* expression in host dorsolateral striatum and *Bdnf* expression in grafted DA neurons. b Confocal micrograph of *Bdnf* mRNA in DA grafted tissue. Cells depicted in (i-iii) are shown at increased magnification in inset (i'-iii'). Scale bars = 100 μ m for panel (b), 10 μ m for inset images. c Percentage of grafted DA neurons expressing *Bdnf* mRNA in Val68Val and Met68Met grafted rats. Mean \pm SEM. Unpaired *t*-test. NOTE: *Bdnf* mRNA data are available from only three Val68Val grafted subjects due to limited tissue sections containing grafts. d,f Micrographs of *Trkb* mRNA expression, presumed to be principally within medium spiny neurons, in grafted and intact dorsolateral striatum of sham grafted (d) and DA grafted (f) rats. Scale bars = 25 μ m. e,g Quantification of *Trkb* mRNA in sham grafted (e) and DA grafted (g) rats depicted in panels

(d) and (f), respectively. Mean \pm SEM. Two-way repeated measures ANOVAs with Šídák's post-hoc test. Abbreviations: ctx = cortex, str = striatum, *Bdnf* = brain-derived neurotrophic factor, *Trkb* = tyrosine receptor kinase B, DA = dopamine, ns = not significant

Author Manuscript

Author Manuscript

Author Manuscript

Author Manuscript

Table 1

Targeted antigens and corresponding antibodies.

Antigen	Assay	Primary antibody	Vendor	Catalog number	Dilution	Secondary antibody ^a
Tyrosine Hydroxylase	TH-VGLUT2-PSD95	rabbit anti-TH	Millipore	AB152b	1:4000	SuperBoost™
Tyrosine Hydroxylase	TH-Synaptopodin and TH-VGLUT1-PSD95	mouse anti-TH	Millipore	Mab318	1:4000	SuperBoost™
Synaptopodin	TH-Synaptopodin	rabbit anti-synaptopodin	Synaptic Systems	163002	1:4000	A21207
PSD95	TH-VGLUT1/2-PSD95	mouse anti-PSD95 IgG2a	LSBio	C150376	1:1000	A21241
VGLUT2	TH-VGLUT2-PSD95	mouse anti-VGLUT2 IgG1	Abcam	Ab79157	1:300	2045303
VGLUT1	TH-VGLUT1-PSD95	mouse anti-VGLUT1 IgG1κ	BioLegend	821302	1:1000	2045303

^aNOTE: Secondary antibody catalog numbers are Alexa Fluor®-conjugated, purchased from Invitrogen®

Table 2

RNA targets and corresponding RNAscope® probes.

RNA Target	Probe	Accession number	Catalog number
<i>Vglut2</i>	Rn-Slc17a6	NM_053427.1	317011
<i>Tph2</i>	Rn-Tph2	NM_173839.2	316411
<i>Bdnf</i>	Rn-Bdnf-CDS	NM_012513.4	409031

Author Manuscript

Author Manuscript

Author Manuscript

Author Manuscript